



DESDE 1902
INSTITUTO DE HIGIENE E
MEDICINA TROPICAL
UNIVERSIDADE NOVA DE LISBOA



UNIVERSIDADE
NOVA
DE LISBOA

Universidade Nova de Lisboa
Instituto de Higiene e Medicina Tropical

3-Dimensional characterization of PanIN (Pancreatic
Intraepithelial Neoplasia) in cleared human pancreatic cancer
tissues by multiplex immunofluorescence

Susana Canastra Dias

DISSERTAÇÃO PARA A OBTENÇÃO DO GRAU DE MESTRE EM CIÊNCIAS BIOMÉDICAS

OUTUBRO, 2019



DESDE 1902
INSTITUTO DE HIGIENE E
MEDICINA TROPICAL
UNIVERSIDADE NOVA DE LISBOA



UNIVERSIDADE
NOVA
DE LISBOA

Universidade Nova de Lisboa
Instituto de Higiene e Medicina Tropical

3-Dimensional characterization of PanIN (Pancreatic
Intraepithelial Neoplasia) in cleared human pancreatic
cancer tissues by multiplex immunofluorescence

Autor: Susana Canastra Dias

Orientador: Mireia Castillo-Martin

Coorientador: Celso Vladimiro Cunha

Dissertação apresentada para cumprimento dos requisitos necessários à obtenção do grau de Mestre em Ciências Biomédicas

Acknowledgements

Para a realização e concretização desta tese vários foram os intervenientes essenciais ao seu normal desenvolvimento, pelo que agradeço profundamente a todos.

To Mireia Castillo-Martin for allowing me to develop this work in her group and for all the scientific knowledge and critical analysis shared with me, during the development of this work, that was essential for my professional and personal development and growth.

Ao Professor Celso Cunha, pela sua contribuição sempre presente e atenta, assim como pela sua simpatia e boa disposição em todos os momentos.

To all the members of Molecular and Experimental Pathology Laboratory, for the scientific discussions and feedback during all the stages of this project.

To the ABBE facility members, especially to Anna Pezzarossa, for the support during data acquisition and analysis.

Ao Paulo Carriço, membro da *Harware Platform*, pela sua pronta ajuda na elaboração do suporte personalizado para as amostras usadas.

Aos meus colegas de trabalho e amigos, Inês Marques, Maria Inês Romano e Sérgio Casimiro, pela sua motivação constante e apoio demonstrado na conciliação do projeto pessoal com a componente profissional. Sem eles a realização deste trabalho teria sido impossível.

Às minhas amigas, Alexandra Martins e Iolanda Martins, pela sua amizade, incentivo e pelos momentos de descontração tão necessários durante esta fase.

Aos meus pais e irmã pelo incentivo constante pela procura e concretização dos meus sonhos e objetivos e pelo seu apoio incondicional, para mim essencial na criação do meu porto seguro.

Ao meu namorado pela sua paciência e suporte em todos os momentos, assim como pela partilha de ideias, discussão de resultados e revisão deste trabalho, que me trouxe uma nova perspetiva e abordagem.

Resumo

O adenocarcinoma pancreático (PDAC) é uma das neoplasias com maior taxa de mortalidade devido à ausência de métodos de detecção precoce e terapêuticas eficazes, levando à sua detecção numa fase avançada e não-tratável da doença. A sua carcinogénese é explicada através da acumulação de alterações moleculares, numa das três lesões precursoras, neoplasia cística mucinosa, neoplasia intraductal papilar mucinosa e neoplasia intraepitelial pancreática (PanIN).

A PanIN é a lesão precursora mais frequente, caracterizada como uma proliferação epitelial não invasiva, que apresenta vários graus de displasia histológica, refletindo as alterações moleculares existentes nas diferentes fases, afetando os genes K-RAS, P16, TP53, SMAD4, entre outros.

A histologia é o *gold standard* para o estudo de amostras, seus componentes e relação anatómica, através do corte das amostras em fatias finas, fornecendo apenas uma perspetiva bidimensional da amostra, que é limitante e que enviesada a perceção e o estudo da tridimensionalidade dos tecidos, em condições normais e patológicas.

De forma a permitir o estudo tridimensional das amostras e evitar os artefactos dados pela reconstituição sequencial de fatias finas têm sido desenvolvidas as técnicas de *clearing*, que através da redução da opacidade dos tecidos, pela homogeneização dos índices refrativos dos vários constituintes celulares, reduzem a dispersão da luz e permitem a sua penetração. Várias são as técnicas até agora descritas, que se agrupam, consoante o reagente usado, em aquosas ou solventes orgânicos, sendo este último grupo mais eficaz em tecidos fibróticos, como os tecidos cancerígenos.

Para a caracterização dos tecidos humanos são necessárias técnicas de imunofluorescência, no entanto a penetração máxima dos anticorpos, até agora descrita para blocos de parafina com PDAC, é de 0.6 mm, devido ao seu elevado conteúdo fibrótico.

O presente trabalho teve como objetivo a otimização das técnicas de imunofluorescência aplicadas a tecidos espessos com PDAC, assim como, o estudo da relação anatómica entre os vários graus de PanIN e o PDAC. Para isso foram utilizados cinco blocos de parafina do arquivo do Centro Clínico da Fundação Champalimaud, com 2 mm de espessura, corados através de imunofluorescência com anticorpos anti-citoqueratina 19, anti-AGR2 e anti-p53.

A otimização das técnicas de imunofluorescência, aplicadas a amostras espessas, foi feita através da introdução de um passo de recuperação antigénica, digestão enzimática e extensão do tempo de incubação do anticorpo, assim como, um aumento da quantidade de anticorpo por amostra, o que permitiu a visualização das amostras em toda a sua extensão. Todas as marcações citoplasmáticas foram desenvolvidas com êxito, no entanto não foi possível identificar marcação nuclear.

Através da análise das amostras branqueadas, coradas com anticorpos anti-citoqueratina 19 e anti-AGR2, foi possível identificar ductos normais, ductos com PanIN e células cancerígenas, no entanto, trabalho adicional é necessário para estabelecer parâmetros de correlação das características apresentadas pelos ductos com PanIN, em amostras

branqueadas espessas, com a classificação histológica. A nível anatómico, identifica-se uma tendência para as células cancerígenas se desenvolverem e localizarem junto das ramificações ductais e não perto dos ductos de maior calibre.

Palavras-chave: Adenocarcinoma do pâncreas, neoplasia intraepitelial pancreática (PanIN), *deep antibody immunolabelling*, técnicas de *clearing*.

Abstract

Pancreatic ductal adenocarcinoma (PDAC) is one of the deadliest types of solid cancer mainly due to the lack of early detection techniques and therapeutic options, which makes its diagnosis and detection usually in advanced and untreatable stage of the disease. Currently it is accepted that its carcinogenesis is based on the accumulation of molecular changes in three precursor lesions, namely mucinous cystic neoplasm, intraductal papillary mucinous neoplasm and pancreatic intraepithelial neoplasia (PanIN).

PanIN is the most common precursor of PDAC and it is characterized as a non-invasive epithelial proliferation in pancreatic ducts, with different degrees of cytological and morphological atypia that reflects a molecular transformation with mutations on K-RAS, P16, TP53 and SMAD4 genes at different stages.

Histology is the gold standard technique for studying tissue specimens, their components and anatomical relationship, which by producing thin sections of tissues, allows a bidimensional analysis that limits and biases the correct tridimensional perspective of normal and pathological situations.

To overcome the limitations presented by the analysis of thin sections, clearing techniques have been developed with the goal to reduce tissue's opacity through the homogenization of refractive indexes within a cell and surroundings, which reduces light scattering and allows its penetration deep in the tissue. Several clearing techniques have been described so far, that can be divided, according to the type of reagent, in solvent-based and aqueous clearing techniques, being the first group more effective with fibrotic tissue, such as tumour samples.

Immunofluorescence techniques are necessary to study human samples, but up until now the maximum penetration of an antibody described in the literature in human paraffin-blocks with PDAC is 0.6 mm, due to the high fibrotic content.

The present work seeks to optimize deep-antibody immunolabelling of thick samples with PDAC and study the anatomical relationship between different grades-PanIN and PDAC. In order to do that, five archival formalin-fixed paraffin-embedded blocks from Champalimaud Clinical Centre were used and stained with anti-cytokeratin 19, anti-AGR2 and anti-p53 antibodies.

The optimization of the immunolabelling was achieved through the application of an antigen retrieval step, enzymatic digestion and an increase of incubation time and amount of antibody, which allowed the visualization of the sample in all its extension. All the cytoplasmic stainings were successful but we were not effective with the nuclear staining.

Through the analysis of cleared samples, stained with anti-cytokeratin 19 and anti-AGR2 antibodies, we could identify normal pancreas, PanIN and PDAC. Nevertheless, additional work has to be done to establish a correlation between the features presented by the ducts of cleared thick samples and the histological grade. Anatomically there's a tendency for cancer cells to develop and deposit next to ductal terminations and not close to ducts with big caliber.

Keywords: Pancreatic ductal adenocarcinoma, pancreatic intraepithelial lesion, deep antibody immunolabeling, clearing techniques.

Table of contents

1. Introduction.....	1
1.1 – Normal pancreas	1
1.2 – Pancreatic ductal adenocarcinoma.....	3
1.3 – Pancreatic intraepithelial neoplasia	4
1.4 – Clearing techniques.....	9
1.5 – Deep antibody immunolabeling protocol in cleared samples	13
1.6 – Objectives	16
2. Material and Methods	18
2.1 – Human samples.....	18
2.1.1 – Ethical approval	18
2.1.2 – FFPE blocks of human pancreatic tissue	18
2.2 – Antibodies optimization on thin sections.....	19
2.3 – Deep immunolabelling optimization on thick specimens.....	20
2.3.1 – AR, with and without presoaking, on 2 mm-thick FFPE blocks	20
2.3.2 – Application of different incubation time and centrifugal forces on normal 2 mm-thick FFPE blocks	21
2.3.3 – Collagenase pretreatment on FFPE blocks with PDAC and a high fibrotic content.....	22
2.3.4 – Validation of anti-p53 and anti-AGR2 antibodies on a 2 mm-thick positive control	23
2.4 – Multiplex in cleared FFPE blocks of human pancreatic tissue.....	24
2.5 – Imaging and data analysis.....	24
3. Results and Discussion	26
3.1 – Definition of antibodies parameters on thin sections.....	26
3.1.1 – Definition of CK 7 and CK 19 expression on ductal epithelial cells.....	26

3.1.2 – Anti-CK 19 antibody [EP1580Y] (Alexa Fluor® 568), anti-AGR2 antibody [EPR3278] (Alexa Fluor® 555) and anti-p53 antibody [SC53394 AF647] (Alexa Fluor® 647) optimization protocol.....	27
3.2 – Influence of AR, enzymatic pretreatment and antibody incubation parameters on thick samples.....	29
3.2.1 – AR for 40 minutes after presoaking increases signal-to-noise ratio.....	29
3.2.2 – Longer antibody incubation favors staining’s homogeneity and intensity .	34
3.2.3 – Type I collagenase digestion promotes antibody penetration on PDAC thick samples.....	37
3.2.4 – Anti-p53 and anti-AGR2 staining on thick positive control specimens	40
3.3 – Multiplex studies in cleared FFPE blocks with PDAC.....	44
3.3.1 – Histological grade and p53 expression	44
3.3.2. – Multiplex on 2 mm-thick samples	45
4. Final Considerations and Future Goals.....	53
5. References.....	56
6. Appendix.....	65
6.1 - Appendix 1 - Risk assessment of reagents	65
6.2 - Appendix 2 - Samples with enzymatic digestion	67
6.3 - Appendix 3 – Sample’s dimension.....	75
6.4 - Appendix 4 – Deep immunolabelling of FFPE with PDAC	76

List of figures

Figure 1 - Anatomical relationship of pancreas and surrounding organs.....	1
Figure 2 - Histological section of a normal pancreas stained with hematoxylin and eosin (HE).....	2
Figure 3 - Histological section of a pancreatic duct stained with HE.....	2
Figure 4 - Histological section of PDAC stained with HE.....	4
Figure 5 - Histological features of PanIN-1A, PanIN-1B, PanIN-2 and PanIN-3 stained with HE.....	5
Figure 6 - Schematic representation of PanIN morphological and genetic progression...	6
Figure 7 - Schematic representation of the two main clearing groups: solvent-based and aqueous clearing techniques.....	10
Figure 8 - Anti-CK 7 and anti-CK 19 (AlexaFluor® 594) antibodies expression in normal pancreatic ducts.....	26
Figure 9 - Anti-CK 7 and anti-CK 19 (AlexaFluor® 594) antibodies expression in PDAC.....	27
Figure 10 - Anti-CK 19 (AlexaFluor® 568) antibody optimization in normal pancreatic ducts.....	28
Figure 11 - Anti-AGR2 (AlexaFluor® 555) antibody optimization in rectal adenocarcinoma.....	28
Figure 12 - Anti-p53 (AlexaFluor® 647) antibody optimization in lung squamous cell carcinoma.....	29
Figure 13 - Heterogeneous staining pattern of a representative section with anti-CK 19 (AlexaFluor® 568) antibody.....	31
Figure 14 – Influence of AR on thick samples from FFPE blocks of normal pancreas.....	33
Figure 15 - Ductal system organization.....	33

Figure 16 - Clearing efficiency with DBE.....	34
Figure 17 - 3D picture from three FFPE blocks of normal pancreas with anti-CK 19 (AlexaFluor® 568) antibody.....	35
Figure 18 – Antibody supply experiment on an entire FFPE block of normal pancreas.....	36
Figure 19 - Enzymatic pretreatment of seven FFPE blocks from the same patient with type I, type IV and type I + type IV collagenase, for 1 hour and 3 hours.....	38
Figure 20 - 3D aspects of the control sample and samples processed before glycine and after blocking for 3 hours with type I and IV collagenase.....	39
Figure 21 - AGR2 expression in three cases of rectal adenocarcinoma.....	41
Figure 22 - Human sample with rectal adenocarcinoma after clearing with DBE.....	41
Figure 23 - Anti-AGR2 expression on a thick sample with rectal adenocarcinoma.....	42
Figure 24 - Human sample with ovarian serous carcinoma after clearing with DBE....	42
Figure 25- Anti-P53 expression on a thick sample with serous carcinoma.....	43
Figure 26 - Anti-AGR2 (AlexaFluor® 488) antibody optimization in rectal adenocarcinoma.....	45
Figure 27 - Macroscopic aspect of the five final samples throughout the protocol.....	47
Figure 28 – 3D overview look of the multiplex with anti-CK 19 and anti-AGR2 antibodies on five samples with PDAC.....	48
Figure 29 – 2D perspective of AGR2 expression in a phenotypically normal duct.....	50
Figure 30 – 3D perspective of normal ductal component, PanIN and PDAC, stained with anti-AGR2 and anti-CK 19.....	50
Figure 31 – 2D perspective of ductal cancerization.....	51
Figure 32 – 3D perspective of ductal branching.....	51

Figure 33 – 2D perspective of cancer cells in close connection to small caliber ducts, corresponding to the terminal ducts.....52

Figure 34 - Schematic workflow of the optimized protocol.....54

List of tables

Table 1 - Summary of the parameters tested during the study of the influence of the AR on immunofluorescence technique results on thick samples.....	20
Table 2- Summary of the parameters tested during the study of the influence of enzymatic pretreatment on antibody penetration on samples with PDAC.....	23
Table 3 - Excitation and emission range in the filterset used for the microscopic evaluation of 5 μ m-thick slices.....	24
Table 4 - Excitation of the laser and filter emission used during imaging acquisition on the Ultramicroscope II (LaVision).....	25
Table 5 - Imaging acquisition parameters for anti-CK 19, anti-AGR2 and anti-P53 antibodies on thick samples.....	25
Table 6 - Summary results of the microscopic observation of two FFPE blocks of normal pancreas (sample 4 and 5) with three different conditions: standard protocol without AR, AR for 40 or 20 minutes with and without presoaking in the AR solution.....	30
Table 7 - Histological grade, p53 expression, location and staging in the 3D analyzed samples.....	44

List of abbreviations

2D - 2-dimensional

3D - 3-dimensional

3DISCO - 3-Dimensional imaging of solvent-cleared organs

ACT-PRESTO - Active clarity technique-pressure related efficient and stable transfer of macromolecules into organs

AGR2 - Anterior gradient 2

AR - Antigen retrieval

BABB - Benzyl-alcohol, benzyl-benzoate

BSA - Bovine serum albumin

CDKN2A - Cyclin-dependent kinase inhibitor 2A

CK - Cytokeratin

CLARITY - Clear lipid-exchanged acrylamide-hybridized rigid imaging/immunostaining/in situ hybridization-compatible tissue hydrogel

CUBIC - Clear, unobstructed brain/body imaging cocktails and computational analysis

DBE - Dibenzyl ether

DCM - Dichloromethane

DMSO - Dimethyl sulfoxide

DPC4/SMAD4 - Deleted in pancreatic cancer 4/Mothers against decapentaplegic homolog 4

ECi - Ethyl cinnamate

ECM - Extracellular matrix

EDTA - Ethylenediamine tetraacetic acid

FF - Formalin-fixed

FFPE - Formalin-fixed paraffin-embedded

GFP - Green fluorescent protein

HE - Hematoxylin and eosin

iDISCO - Immunolabeling-enabled three-dimensional imaging of solvent-cleared organs

MUC - Mucin

PACT - Passive CLARITY technique

PanIN - Pancreatic intraepithelial neoplasia

PARS - Perfusion-assisted agent release *in situ*

PBS - Phosphate buffered saline

PDAC - Pancreatic ductal adenocarcinoma

PFA - Paraformaldehyde

RI - Refractive index

sDISCO - Stabilised 3-dimensional imaging of solvent-cleared organs

SDS - Sodium dodecyl sulfate

SeeDB - See deep brain

SWITCH - System-wide control of interaction time and kinetics of chemicals

THF - Tetrahydrofuran

uDISCO - Ultimate dimensional imaging of solvent-cleared organs

1. Introduction

1.1 – Normal pancreas

The pancreas is located in the retroperitoneum, behind the left hepatic lobe and the stomach. It can be divided anatomically in head, body and tail, where its head lies in the duodenal curve and the tail ends near the hilum of spleen (Figure 1). Due to its location, diagnose of pathological conditions and development of therapeutic procedures are difficult. It measures between 14 to 20 cm, weights around 100 g and macroscopically presents a pink-pale color and packed angulated lobules (1).

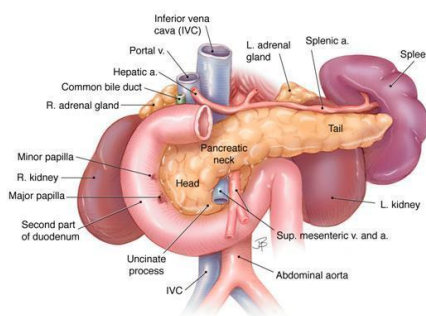


Figure 1 - Anatomical relationship of pancreas and surrounding organs. From <https://www.pancreapedia.org/reviews/anatomy-and-histology-of-pancreas>, 23 of January 2019.

It is composed by an endocrine and an exocrine component. The first is composed by the islets of Langerhans, responsible for the glucose metabolism and the second is composed by acinar cells that produce digestive enzymes (Figure 2).

The exocrine component is composed by acinar cells that will drain their enzymatic production to the duodenum, by the main pancreatic duct, or duct of Wirsung, through the Ampulla of Vater and from the Santorini's duct to the minor ampulla, in the superior part of pancreas head (1).

Histologically, acinar cells comprise 85% of pancreatic content, presenting a pyramidal shape and basal nucleus, arranged in rounded nests with a central lumen, normally not visible (Figure 2).

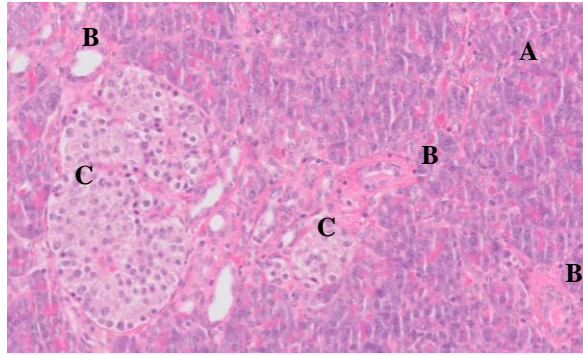


Figure 2 - Histological section of a normal pancreas stained with hematoxylin and eosin (HE). Normal pancreas is composed by acinar cells (A), with a pyramidal shape arranged in round nests, pancreatic ducts (B), composed of cuboidal epithelial cells, and islets of Langerhans (C), characterized by a smooth but well defined contour of reticular fibers, surrounding a round shape-group of loose cells, paler than the exocrine content. Original picture (20x).

In the lumen of acinar clusters begins the ductal system with centroacinar cells that join the intercalated ducts, composed by low cuboidal epithelial cells. These ducts will converge into bigger ducts, the intralobular ducts and then interlobular ducts, composed by columnar epithelial cells that will converge in the main and accessory pancreatic duct. Ducts with bigger calibre can be surrounded by fibrous tissue, but not by smooth muscle (Figure 3). Besides collecting the digestive enzymes, the ducts secrete a buffer composed with water, chloride and bicarbonate that will stabilize the protoenzymes secreted by acinar cells (1).

All ducts are positive for low molecular weight cytokeratins (CKs) 7, 8, 18 and 19. Also, some specific mucin (MUC) expression is seen: MUC6 stains in centroacinar cells and intercalated ducts and MUC1 stains in small intralobular and intercalated ducts. MUC2 and MUC5AC are not normally present (1).

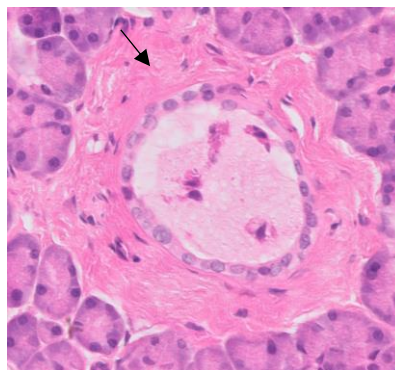


Figure 3 - Histological section of a pancreatic duct stained with HE. Picture shows a pancreatic duct in the center, with cuboidal cells, surrounded by fibrous tissue (arrow). Original picture (40x).

1.2 – Pancreatic ductal adenocarcinoma

Pancreatic ductal adenocarcinoma (PDAC) accounts for more than 95% of pancreatic exocrine malignancies (2), being one of the deathliest epithelial malignancies (1). Around 60-70% of the cases develop in the pancreatic head (3,4). It has poor prognosis and high mortality rate, almost matching its incidence, mainly due to its late detection as an advanced and untreatable disease (1).

The prevalence of PDAC increases with age (5) and it's associated with risk-factors, such as smoking, alcoholism, diabetes mellitus, obesity and chronic inflammation (4). A small percentage, around 10%, are associated with familiar-risk (1,3,4,6).

Most patients present symptoms at a late stage of the disease, and often they are non-specific such as epigastric pain, fatigue, weight loss, nausea, jaundice and symptoms associated with biliary obstruction, such as dark urine and pruritus (1,3,4). In the late stage of the disease, Sister Mary Joseph nodule can be present as a palpable periumbilical nodule, representing a subcutaneous metastasis (1).

It can be diagnosed with computerized tomography, magnetic resonance imaging and endoscopic ultrasound (1,3,4). Surgery represents the main form of treatment for localized tumors, and although most of the cases are resistant to conventional chemotherapy and radiotherapy, advanced tumors are treated systemically (6).

Histologically, PDAC presents infiltrative cuboidal cells with bizarre cellular shape with enlarged and pleomorphic nuclei, arranged in a glandular pattern (Figure 4). It is often surrounded by a fibrotic stroma, named desmoplastic reaction, composed by fibroblasts, collagen fibres and inflammatory cells. Sometimes necrosis can be observed in the glandular lumen (1).

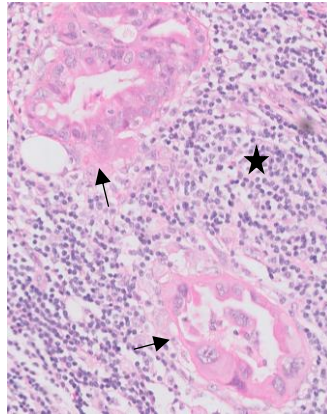


Figure 4 - Histological section of PDAC stained with HE. Bizarre cells (arrow) in glandular pattern are seen, with pleomorphic and enlarged nuclei, in which a prominent nucleolus is present, surrounded by a high inflammatory content (star). Original picture (20x).

Cancer-associated fibroblasts and activated pancreatic stellate cells are responsible for the extracellular matrix (ECM) production, that forms a 3-dimensional (3D) non-cellular network that diminishes drug delivery. Type I collagen, produced by pancreatic stellate cells, is the most abundant component in ECM and the main responsible for the desmoplastic reaction in the interstitial space (7,8). Additionally, PDAC cells produce type IV collagen that deposits around the cancer cells, forming basement membrane-like structures. Collagen function as signaling molecules or ligands for integrin receptor in PDAC cells has been described, promoting proliferation, migration and cellular viability (7,8).

It is currently accepted that the formation of PDAC is based on a gradual process arising from one of the three known precursor lesion: pancreatic intraepithelial neoplasia (PanIN), intraductal papillary mucinous neoplasms and mucinous cystic neoplasms (1,9).

1.3 – Pancreatic intraepithelial neoplasia

PanIN is an asymptomatic, non-invasive lesion in the intralobular pancreatic ducts, that measures up to 5 mm (10). It's not detected with imaging techniques due to its small size, so histological techniques are the gold-standard for its diagnosis (11). It's thought to be the most common precursor lesion of PDAC and its progression takes around 11.7 years (1,12). This progression model is accepted since most of the PDAC harbor the

same genetic abnormalities as surrounding PanIN (13,14). Besides, the prevalence increases with age in both PanIN and PDAC and the amount of PanIN is higher in samples with PDAC than normal pancreas (5,15).

Makohon-Moore and colleagues presented three possible scenarios for the progression model: a) PanIN and PDAC arise independently; b) they share a common ancestral cell but different genetic events causes evolution of PDAC; c) they share a common ancestral cell that already has all alterations required to form a malignant disease. By analysing the whole-exome sequencing and phylogenic relationship between PDAC and their anatomically distant PanINs, evidences point to an emerging of a PDAC from a pre-existing PanIN lesion and that a single mutant cell has the ability to spread through the ductal system to generate a new lesion (12).

For decades, this lesion had different classifications but a consensus was proposed by Hruban *et al.* (2001), which classified it as PanIN and divided it in three groups, according to its cytological and architectural alteration: PanIN-1, PanIN-2 and PanIN-3 (16).

PanIN-1 represents a lesion with basal nucleus with low nuclear atypia of columnar or cuboidal cells in a flat (1A) or papillary conformation (1B). PanIN-2 is a flat or papillary lesion with cytological atypia, with loss of polarity, nuclear crowding, hyperchromasia, pleomorphism and pseudostratification, but rare mitosis. PanIN-3, also referred as carcinoma *in situ*, represents a papillary lesion with nuclear atypia, such as macronucleoli and abnormal mitotic features (Figure 5) (1,17). In none of these lesions basement membrane is invaded, as happens in adenocarcinoma (1,11,15,18,19).

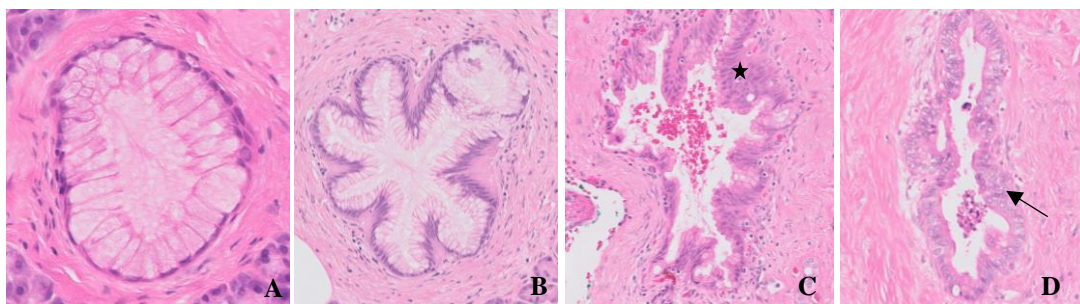


Figure 5 - Histological features of PanIN-1A, PanIN-1B, PanIN-2 and PanIN-3 stained with HE. A and B - PanIN-1A (A) presents low nuclear atypia with a basal nucleus and a flat lesion, that will present a papillary conformation in PanIN-1B (B). C - PanIN-2 with nuclear atypia, such as hyperchromasia, nuclear crowding and pseudostratification (star). D - In PanIN-3 several mitosis are seen in the atypical nucleus (arrow). Original picture (A - 40x, B - D - 20x).

A new classification system arose due to the questionable clinical relevance of PanIN-1 and PanIN-2, which proposed a two-grading system: low-grade PanIN, which includes the former PanIN-1 and 2, and high-grade PanIN, with PanIN-3 (20).

The morphological progression, of low-grade to high-grade PanIN, reflects the presence of several and gradual molecular alterations of cells that will lead to its transformation in an invasive carcinoma (9,13,15,21–24) (Figure 6). These mutations occur in oncogenes and tumour suppressor genes, which will lead to genetic deregulation and an uncontrolled growth of cells (15,25).

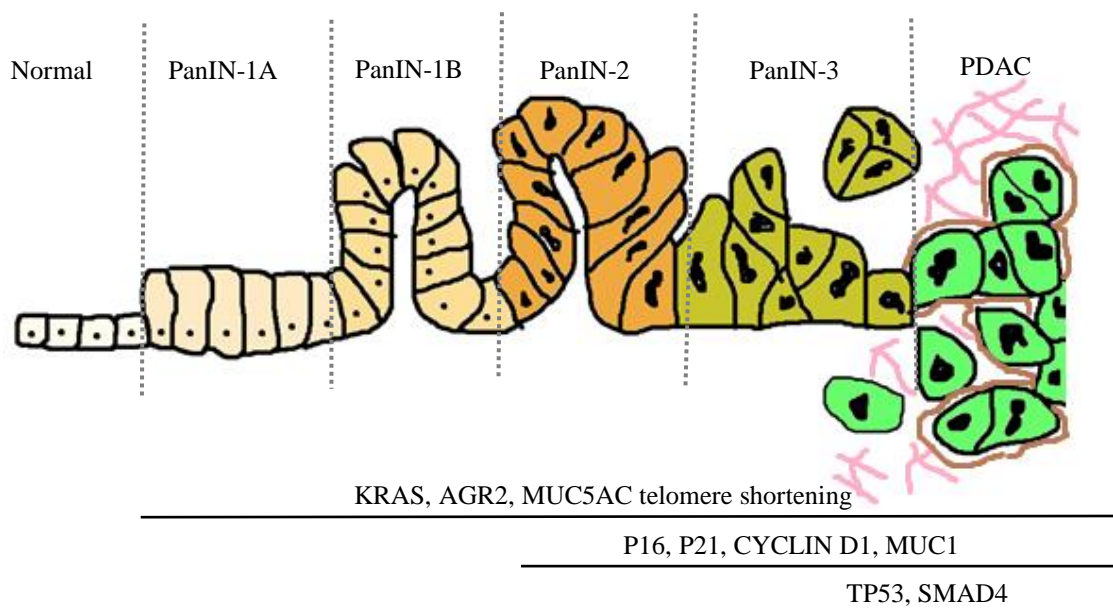


Figure 6 - Schematic representation of PanIN morphological and genetic progression. KRAS mutation, telomere shortening and expression of MUC5AC and AGR2 are early genetic events, followed by inactivation of P16, overexpression of P21, CYCLIN D1 and MUC1. TP53 mutation and SMAD4 are late genetic events. Desmoplastic reaction is found in PDAC, being composed by type-I collagen in the interstitial space (pink) and type-IV collagen surrounding cancer cells (brown). Original figure.

One of the earliest events is KRAS mutation (13,15), an oncogene that's involved in Mas/Mapk pathway which regulates cell-growth, survival and proliferation (15,24). The most common mutation occurs in codon 12, which causes a constitutive activation of the protein, but mutations in codon 13 and 61 can also occur (10,26). More than 90% of all grade PanIN and PDAC harbor mutation in codon 12, although the amount of cells mutated increase with the grade (10,14,27). This mutation is thought to be one of the main and first events to this progression. Animal models were produced with mutation in codon 12 of exon 1 of KRAS in a Pdx1-Cre transgene animal (11). In these animals, histological lesions similar to low and high-grade PanIN were observed, which

progressed with the aging of the animal (11,19,28). Besides, occurrence of PDAC was observed after a long latency, and when combined with other mutations, such as in TP53, a higher frequency and faster progression were observed (15,19,24,28). KRAS activation turns-on other signalling cascades, so its alteration has a deregulation effect in the downstream molecules, such as Egfr, Tgf- β , Wnt, Notch, Mothers against decapentaplegic homolog (Smad) and others (25).

Telomeric instability is another early event in this carcinogenesis, being present in over 90% of PanIN (29). Telomeres represent protective repetitive DNA sequences at the end of chromosomes. This shortening causes chromosomal instability that will lead to abnormal numerical and structural division of chromosomes, meaning that this instability has power to trigger the genetic alterations.

Inactivation of tumour suppressor genes cyclin-dependent kinase inhibitor P16/cyclin-dependent kinase inhibitor 2A (CDKN2A) is also observed in 30%, 55%, 70% and 95% of PanIN-1, PanIN-2, and PanIN-3 and PDAC, respectively (13,24,30). P16 is located in chromosome 9 and its protein inhibits the association between CDK4 and CDK6, and consequently their association to Cyclin D1, causing cell-arrest in G1-S phase. P16 inactivation can occur through homozygous deletion, intragenic mutation and loss of the remaining allele or promotor hypermethylation (30,31).

Anterior gradient 2 (AGR2) is thought to be a member of the disulphide isomerase protein, due to the present of an endoplasmic reticulum leader sequence, functioning in protein maturation, such as MUCs (32–35). It's one of the Tgf- β downregulated genes and it's involved in endoplasmic reticulum stress (36). Its presence in PDAC promotes cancer proliferation, resistance and survival. It's expressed in all PanIN grades and in 98% of PDAC, but different staining intensity can be observed (32,35,36).

Other early mutations are seen in P21, MUC1,3,5AC and HER-2, that are followed by mutations in CYCLIN D1 and CYCLOOXYGENASE (15,37).

P21 is a protein that inhibits CDK activity, interfering with Cyclin E/CDK2 complex, which will control cell-cycle progression. An overexpression of p21, that follows the PanIN progression, is observed in 9% of normal ducts, 16% PanIN 1A, 32% PanIN 1B,

56% PanIN 2, 80% PanIN 3 and 85% PDAC and it causes overexpression of CYCLIN D1, that is detected in 60% of PDAC (38,39).

With PanIN progression, other mutations appear, such as in TP53, SMAD4, MUC4, BRAC2, KI-67 genes (22,28,40).

TP53 is a tumor suppressor gene that encodes a transcription factor involved in cell-cycle arrest (G1-S) and apoptosis. It's located in chromosome 17 and it's a checkpoint protein that enables either DNA repair or induces apoptosis. When mutated, this protein is more stable which allows its detection with immunohistochemistry techniques (15,39). It's mutated by point-mutations, intragenic frameshift deletions, allelic loss (27). This mutation is present in 50 to 75% of PDAC (27,41,42).

Another late event in this carcinogenic pathway is mutation of DPC4 (Deleted in Pancreatic Cancer)/SMAD4 gene (15) . It is quite specific for pancreatic cancer, although it can also be present in colon, breast, ovarian and bile duct cancers. The SMAD4 is a tumour suppressor gene, present in chromosome 18, that belongs to the family of SMADs, which are intracellular mediators of transcriptional responses to Tgf- β (43). It is a heterodimer, formed by the phosphorylate status of Smad2 and Smad3, that will act as a transcription factor in genes related to growth inhibition and apoptosis (15). Smad4 is detected by immunohistochemistry, where its expression accurately reflects the gene status. In this case, mutation causes gene silencing, due to a homozygous deletion or intragenic mutation with loss of the second allele (43). Some conflicting results are exposed on the literature about its presence, by immunohistochemistry, some pointing its preservation in high-grade PanIN (44,45) and other pointing to its loss in around 30% of high grade-PanIN and 55% to 66% in PDAC (22,41,46). This heterogeneous results could be related with gene status alteration when in presence or absence of carcinoma (45).

Alterations in MUC expression have also been reported during the progression from PanIN to PDAC. MUC1 is expressed in normal pancreatic ducts and acini and is responsible for the lumen formation. It loses expression in low-grade PanIN but it's highly expressed in high-grade and invasive carcinoma (25,46). On the opposite side, MUC5AC is not present in normal epithelium but its present in PanIN and PDAC.

Finally, Fanconi anemia family genes can also be altered in PDAC and are related to hereditary cancer susceptibility. Although mismatch repair genes can have a great influence in the tumorigenesis, leading to microsatellite instability it's a rare event in PDAC representing less than 5% of these cases (15).

1.4 – Clearing techniques

Biological tissue's composition is diverse and complex, consisting of different types of cells, fluids and biomolecules, that are linked in a very intricate and organized way (47,48). Being aware of its complexity and structure is essential to understand all the processes and cellular relationships underlying normal and pathological conditions (49).

Conventional histological techniques are, up until now, the gold standard in the anatomical and structural studies of tissues. With this technique, a piece of tissue is cut in thin sections that will be stained and microscopically analyzed to infer and understand, from a 2-dimensional (2D) perspective, its composition, organization and cellular distribution in a 3D context (47,50–53). Although it is the gold standard in pathology for diagnostic (47), conventional histology limits the study of the tissue's tridimensionality (54). Obtaining a 3D image from 2D analyses is feasible, but it's very laborious, time-consuming and error-prone, and it may cause some distortion and loss of information (50,53).

On the other hand, the analysis of a thick sample is limited by its opacity, given by the heterogeneity of refractive indexes (RIs) between the high water content, with a low RI of 1.33, the lower content of proteins, with high RI of 1.44, and lipids, with the highest RI of 1.45. This RI differences, between hydrophobic and hydrophilic regions, promotes lateral light scattering, that combined with absorption by the heme group, melanin and lipofuscin, restricts light diffusion through the tissue, with loss of excitation and emission power, limiting its imaging to only a superficial portion.

RI represents the ratio between the speed of light in a medium relative to its speed in vacuum. This means that every time light faces differences in RI, it changes its speed and direction, reducing its diffusion depth in the tissue (47,49).

Clearing techniques were developed with the goal of decreasing the differences between heterogeneous RI, causing a reduction of light scattering and increasing light penetration in the tissue (47,52,55). Together with the improvement of volume fluorescence microscopy, data acquisition and storage, they opened access to thick samples observation and thus 3D analysis of tissues (49,53,56,57).

Although the main goal of all clearing techniques is the homogenization of RI, they can be divided in solvent-based and aqueous clearing techniques, according to the type of reagent used (Figure 7) (47).

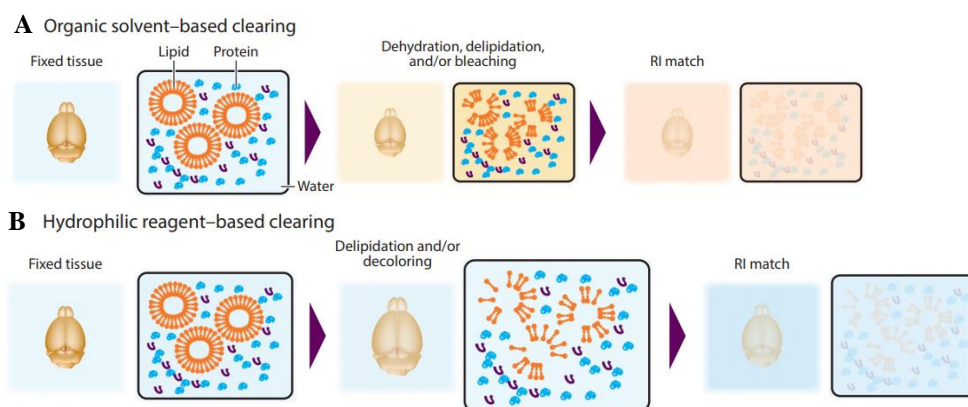


Figure 7 - Schematic representation of the two main clearing groups: solvent-based and aqueous clearing techniques. A – Organic solvent-based protocols have three main steps: dehydration to reduce water content, delipidation with organic solvent to remove lipids (the major source of scattering) and RI matching step, in which sample is emerged in a high RI solution. B – Aqueous clearing protocols, on the other side, don't have a dehydration step, causing hyperhydration which leads to sample's expansion. Delipidation is made through the application of detergents such as triton x100, sodium dodecyl sulfate (SDS) and RI matching solution have in general lower RI than in the organic solvent. From: Tainaka, K., Kuno, A., Kubota, S. I., Murakami, T., & Ueda, H. R. (2016). Chemical Principles in Tissue Clearing and Staining Protocols for Whole-Body Cell Profiling. *Annual Review of Cell and Developmental Biology*, 32(1), 713–741.

They were developed last century, with the work from Werner Spalteholz in 1991, who studied coronary arteries and tried to clear muscle with a mixture of benzyl alcohol and methyl salicylate. From that moment, several modifications and new protocols have been developed to different organs and species (47,49,53,55,56,58–60).

Based on Spalteholz's method, Dodt *et al.* (2007) developed a new method with BABB (benzyl-alcohol, benzyl-benzoate) which enabled a fast clearing of brains from thy1-GFP (Green Fluorescent Protein)-M transgenic mice, mice embryos and *D. melanogaster*, however, it quenched endogenous fluorescence signal and it wasn't very effective in myelinated tissues (49,61).

To overcome this disadvantage, Ertürk *et al.* (2012) developed a new clearing protocol named 3-DISCO (3-Dimensional imaging of solvent-cleared organs), which uses tetrahydrofuran (THF) as dehydration agent, instead of alcohol, and dibenzyl ether (DBE) instead of BABB, as RI matching solution. This allowed imaging of astrocytes and microglia during regeneration/degeneration process in transgenic mice expressing GFP in the brain (49,59). Besides, it was useful for other tissues such as lung, spleen, lymph node, mammary gland and tumor tissues (59). Although it improved the preservation of endogenous signal, there was still loss over time. Then, uDISCO (ultimate DISCO) was developed by Ertürk's group, with a final RI of 1.579. In this protocol, endogenous signal was better preserved thanks to the substitution of THF by *tert*-butanol, as dehydration agent, and by the usage of diphenyl ether, BABB and vitamin E, to prevent oxidation, with good results in brain, internal organs and calcified bones (51). Also, a size reduction in mice volume up to 42% was achieved, allowing complete 10-mm depth scans from dorsal and ventral sides of Thy1-GFP-M mice. Besides, this protocol is compatible with immunohistochemistry protocols and with 1mm-thick human brain tissues, fixed for different periods of time in 4% formalin (51).

Although several organic-solvent clearing protocols are available, they share the main steps. Dehydration, to remove water content from the tissue (since water has lower RI when compared with cellular components such as proteins and lipids); delipidation, to remove the lipid content, since it is one of the main sources of light scattering (49), producing a dehydrated protein-rich content, with a RI higher than 1.5, that will be finally matched with the RI matching step (53,59). Therefore, the ideal organic solvent should have a high lipid solvation ability and a high RI, ranging from 1.56-1.57 (47,53,61).

These methods are very easy to implement, are very fast and versatile, producing good results in a variety of tissues, including fibrous tissue (62), but they are not compatible with lipid staining and can cause some fluorescence fading (55,57) due to the removal of the water content (47,50) and by the formation of peroxides and aldehydes from RI-matching agent. To solve the quenching related to the peroxides and aldehydes formation, in sDISCO (stabilised DISCO) a purification step was added, with column chromatography and applied propyl gallate, an anti-photobleaching, in order to stabilize EGFP signal causing its preservation for over a year after the clearing protocol (55).

Additionally, organic-solvent methods cause tissue shrinkage which can be an advantage when dealing with large samples, since the imaging chamber space is limited (51). With exception of ethyl cinnamate (ECi), that's a non-toxic organic solvent, all the other methods must be handled with care since they use toxic and carcinogenic reagents (63).

Aqueous-based clearing techniques emerged to overcome the main disadvantage of organic-solvent techniques, quenching of endogenous fluorescence (50,53,57). Several principles to achieve transparency may be used, dividing these techniques into three groups:

- High RI matching solutions: It includes all the protocols that immerse samples in high concentrations of sucrose, fructose, glycerol or 2,2'-thiodiethanol, with a RI of 1.4, such as SeeDB (See deep-brain), FRUIT or FocusClear. Here, the delipidation step is substituted by the exchange of every liquid in the tissue for a high RI solution, as the one presented by lipids (47,53,64).
- Hyperhydration: This group acts in two ways: in one side they promote delipidation, with glycerol, detergents and aminoalcohols, and on the other side a hyperhydration, to reduce RI, with urea or formamide, as described in Scale, CUBIC (clear, unobstructed brain/body imaging cocktails and computational analysis) and ClearT, reaching a final RI of 1.38 to 1.48 (47,53,64). In CUBIC protocol, by the usage of aminoalcohols, decolorization power is higher, which is relevant in hematic samples (65). CUBIC protocol uses hyperhydration and high RI sucrose-based clearing solution to accelerate the clearing process (53). Additionally, it achieves delipidation with high concentration of triton (50%) (49,50). The main inconvenient of CUBIC is that it may lead to some protein loss (between 24 and 41%) which may compromise immunostaining (53).
- Hydrogel embedding: This last group makes a chemical transformation of a normal tissue to a hydrogel polymerized-tissue, which will provide physical support and integrity during the delipidation step, with a strong detergent like SDS, to eliminate the main source of scattering, while maintaining the normal morphology and protein content (50,57). Delipidation can be a passive or active process, with the application of an electric field, as described in CLARITY

(clear lipid-exchanged acrylamide-hybridized rigid imaging/immunostaining/*in situ* hybridization-compatible tissue hydrogel), ACT-PRESTO (active clarity technique-pressure related efficient and stable transfer of macromolecules into organs) and PACT/PARS (passive CLARITY technique/perfusion-assisted agent release *in situ*) (49,50,53,57), but no elimination of the ECM is observed with these techniques. The final RI in this group is 1.33 to 1.47 (47).

Aqueous-based techniques are very diverse but they all present good results in preserving the endogenous fluorescence. Although they normally require longer clearing time and sometimes show limited clearing ability (50), they normally lead to an increased specimen's size (49,56). The reagents used are less toxic than in organic-solvent methods and most are easy to implement, except from CLARITY-related techniques where specialized devices, such as an adapted electrophoretic chamber, are necessary (47,64).

1.5 – Deep antibody immunolabeling protocol in cleared samples

Immunohistochemistry is a technique based on the specific antigen-antibody binding ability, commonly used to characterize cellular populations, distinguish between different cellular subtypes, being applied in scientific research and in the clinical context for diagnosis, prognosis and prescription of targeted therapies (66).

Staining large samples with consistent and homogeneous antibody penetration is still a challenge, due to the inversely proportional diffusion rate of antibodies to the sample's thickness. This fact limits labeling of central layers and leads to heterogeneous staining, that will be biased and will limit the analysis. To overcome this issues long incubation periods and specific protocols are often required (50,52,59,67).

Most of the clearing methods are compatible with immunofluorescence techniques, which add important phenotype information on the cellular content, especially to human samples and samples processed with organic solvent, because they can recover the information lost from the fluorescence quenching.

Several improvements have been described to increase antibody penetration in thick samples, such as the use of chemical components that increase permeability of tissues and the application of physical forces to promote antibody penetration. Increasing membrane permeability is important to increase antibodies penetration and normally it is achieved by loss of lipid content (47).

Renier *et al.* (2014) published a method for deep-immunolabelling compatible with 3DISCO, called iDISCO (immunolabeling-enabled DISCO). In this protocol, nonionic detergents and rounds of solvent-based dehydration-rehydration are applied to remove lipids, increasing permeabilization (68). Moreover, methanol, H₂O₂, glycine and heparin are used to reduce endogenous fluorescence and decrease background (47,49,68). Out of 28 antibodies tested, some did not present good results with methanol denaturation pre-treatment, so the authors also described a specific protocol for those methanol sensible-antibodies (68).

This protocol was applied and modified by Nöe *et al.* (2018), in human normal pancreatic tissue and in PDAC, from fresh and formalin-fixed (FF) paraffin-embedded (FFPE) blocks. To increase the penetration depth, a centrifugal force was applied during antibody incubation, sided by an increasing antibody's concentration through the incubation days (69). Besides, enzymatic cleavage of the secondary antibody, to produce single domain antibodies, has been performed to reduce its size and facilitate its dispersion (47,69). With this technique they were able to detect positive staining for CK 19 in 0.7 mm to 1.5 mm depth in normal tissue and 0.3 mm to 0.6 mm in adenocarcinoma cases (69).

In vDISCO they analyzed cleared entire rodent bodies, by increasing the signal-noise ratio of the endogenous signal through the application of pressure and usage of nanobodies, which are smaller (15kDa) than conventional antibodies (150 kDa), conjugated with Atto dyes, that are more photostable and brighter than AlexaFluor®. Simultaneously, to increase penetration they used a mixture of triton X-100, methyl- β -cyclodextrin and trans-1-acetyl-4-hydroxy-L-proline, causing the extraction of cholesterol from cellular membranes and loss of the collagen mesh (54). To reduce autofluorescence, antibodies had emission peaks in the far-red. Aminoalcohol and ethylenediamine tetraacetic acid (EDTA) were applied to reduce background caused by

residual blood and to decalcify bones. Through this technique they were able to construct the first whole-body neuronal connectivity map of a Thy1-GFP-M transgenic mouse (54).

The idea of using smaller antibodies were already brought by Treweek *et al.* (2015), in the PACT protocol, where they used Fab antibodies (70).

CLARITY protocol has also shown improved penetration due to the lipid removal from the polymerized-hybrid, which reduces lipid barrier and allows multiple rounds of immunolabelling (57), although some authors refute the preservation of integrity and protein content through several rounds (48).

To overcome the long protocol for the immunolabeling described in CLARITY, Lee *et al.* (2016) developed ACT-PRESTO, a CLARITY-based clearing technique in which they applied pressure or centrifugal forces to increase the antibody penetration, especially in protein-enriched connective tissues/ECM, where they were able to detect staining in 120µm-depth kidney samples after 3 hours (50). This protocol is compatible with tissues that did not suffer any lipid removal.

Although hydrogel embedding and lipid removal create bigger pores in the tissue, immunolabeling distance seems better in FF non-hybridized tissues (56). Additionally, SDS application in FF tissues does not seem to lead to protein loss. Based in these findings, Lui *et al.* (2017), developed a new method, FASTClear, a combination between CLARITY (SDS delipidation) and iDISCO (detergent permeabilization) to myelinated regions (56). The use of SDS would decrease lipid content and act as an antigen retrieval (AR) solution, due to its denaturant characteristics (56). In this protocol, authors applied a daily supplement of antibody to reduce its trapping on the tissues' surface. This protocol was tested with success in FF 1 cm-thick human brain blocks. FASTClear protocol was later applied by Perbellini *et al.* (2017) to human and canine miocardiac tissue with also good results (52).

The application of AR is also seen in the work published by Saritas *et al.* (2018), where they used citric buffer to improve antibody binding in 1 to 2 mm-thick or whole mouse kidney (71).

From the Chung lab, two protocols to improve antibody penetration have been developed: SWITCH (system-wide control of interaction time and kinetics of chemicals) and stochastic electrotransportation. The first was developed by Murray *et al.* (2015), and is based on the ability to chemically control the interactions and reactions between the tissue and the reagents by two conditions: Switch-on, where a proper buffer is added to promote chemical reaction between the tissue and the reagent, and Switch-off, that prevents any interaction between the target biomolecule and the chemical produced by changes in the solution's pH or composition (48). In this protocol fixation with glutaraldehyde, a small non-ionic crosslinker, with high penetration rate is used to increase stability and integrity of the tissue and its antigenicity during physical and chemical treatments. They were able to perform 22 rounds of antibody labelling in postmortem human tissue, with loss of 3-5% of proteins. Not all the 22 rounds produced good results, but it was not related to loss of antigenicity or integrity (48).

The second, stochastic electrotransportation protocol, was developed by Kim *et al.* (2015). It is based on the application of a rotational electric field, that presents faster diffusion speed and bigger dispersion than simple diffusion and static electric field, without any deformation of the tissue (67). With this approach they were able to reduce incubation periods, but presented better results with CLARITY than with iDISCO and CUBIC (67).

Besides all these modifications and specific protocols, most of the authors do incubations above room temperature to accelerate the reaction and antibody dispersion (48,70). Nevertheless more efforts are necessary to increase the penetration on thick samples, especially in tumor samples (69,72).

1.6 – Objectives

Taking into account the current knowledge on 3D imaging and its limitations, as well as the need to better characterize PDAC precursor lesions, with the development of the present work we seek to:

- Understand if there is a continuum between different grades-PanIN;
- Understand what's the 3D and anatomical relationship between PanIN and PDAC.

Additionally to the two goals mentioned above, we also set the technical goal to:

- Improve deep antibody immunolabelling protocol for FFPE blocks with PDAC, increasing antibody penetration, signal intensity and staining homogeneity.

From the achievement of these three goals we would be able to phenotypically characterize the ductal system from normal ducts to PanIN and PDAC, with anti-CK 19, anti-AGR2 and anti-p53 antibodies, allowing the anatomical study of these entities and their spatial relationship.

2. Material and Methods

2.1 – Human samples

2.1.1 – Ethical approval

This project was submitted and approved by the Champalimaud Foundation's Ethics Committee, since FFPE archival blocks with human material were needed for the development of this work. Samples corresponding to PDAC were identified by a pathologist, irreversibly anonymized and no clinical information was used.

2.1.2 – FFPE blocks of human pancreatic tissue

For the study of the 3D relationship between PanIN and PDAC, seventeen FFPE archival blocks with pancreatic tissue, excised at the Champalimaud Clinical Centre in the past four years, were microscopically analysed by a pathologist to validate the presence of both PDAC and PanIN. Only five FFPE blocks fulfilled this criterion, being the ones used on the multiplex and 3D analysis.

Their p53 expression was assessed with anti-p53 antibody (Clone DO-7, PA0057, Leica) automatically stained in the BOND III Instrument (Leica Biosystems).

Briefly, samples were dewaxed and hydrated. Then AR was made for 20 minutes with AR pH 9 solution and endogenous peroxidase was blocked for 10 minutes. Primary antibody incubation was done for 15 minutes, at room temperature. Post primary antibody was applied for 8 minutes, before the incubation of the polymer for 8 minutes. Development with DAB was done for 10 minutes. Slides were counterstain with hematoxylin. All washes were made using Bond wash solution.

2.2 – Antibodies optimization on thin sections

5 µm-thick slices were obtained in the microtome (HM340E, Thermo Scientific), collected onto a SuperFrost® Plus slide (ThermoScientific) and placed in the oven (Binder), for 20 min at 72°C, before dewax and hydration.

Next, AR was performed with pH 9 AR solution (RE7119, Leica), for 30 minutes at 90°C in a pre-heated steamer (Jata electro). Then, permeabilization of cells was made for 30 min with 0.2% Triton X-100 (X100, Sigma)/1x phosphate buffered saline (PBS, Fisher Bioreagents™) (0.2% PBS-T), followed by a blocking step with 0.5mg/ml bovine serum albumin (BSA) (BP9701-100, Fisher Bioreagents™)/1% Tween 20® (BP337-500, Fisher Bioreagents™)/1x PBS for 20 minutes.

The following antibodies and dilutions were tested:

- Anti-CK 7 antibody (clone RN7, PA0942, Leica), ready to use;
- Anti- CK 19 antibody (clone b170, PA0799, Leica), ready to use;
- Anti-CK 19 Alexa Fluor® 568 conjugated antibody (clone EP1580Y, ab203445, Abcam), dilution 1/200 and 1/400;
- Anti-AGR2 Alexa Fluor® 555 conjugated antibody (clone EPR3278, ab215293, Abcam), dilution 1/50, 1/100 and 1/200;
- Anti-p53 Alexa Fluor® 647 conjugated antibody (clone DO-2, SC53394 AF647, Santa Cruz Biotechnology), dilution 1/50, 1/100 and 1/200.

All CKs were tested in human pancreatic sections, AGR2 was tested in human rectal adenocarcinoma and p53 was tested in human lung squamous cell carcinoma.

For the non-conjugated antibodies, incubation was done for 1 hour and secondary antibody incubation was done for 30 minutes with donkey anti-mouse AlexaFluor® 594 (A21203, Invitrogen), both at room temperature. For the conjugated antibodies, incubation was done overnight at 4°C, skipping the secondary antibody incubation.

Then, incubation with absolute ethanol, followed by incubation with 4% paraformaldehyde (PFA) (Sigma) was done both for 10 minutes. Washes were made

with 1x Bond Wash Solution (AR9590, Leica). Slides were mounted with Prolong™ Diamond Antifade Mountant with DAPI (P36962, Invitrogen).

2.3 – Deep immunolabelling optimization on thick specimens

2.3.1 – AR, with and without presoaking, on 2 mm-thick FFPE blocks

The protocol developed was based on the reported by Nöe *et al.* (2018). Two FFPE blocks of normal human pancreas were divided into three fragments with around 0.5 cm x1 cm and 1 mm thick. Each piece underwent different conditions: no AR, AR without presoaking and AR with presoaking for 24 hours in the AR solution. In each block, two different AR times were tested: 20 minutes and 40 minutes. Experimental groups with the different treatments are summarized in Table 1.

Parameters	20 minutes			40 minutes		
	No AR	AR without presoaking	AR with presoaking	No AR	AR without presoaking	AR with presoaking
Sample	One third of sample 5	One third of sample 5	One third of sample 5	One third of sample 4	One third of sample 4	One third of sample 4

Table 1 - Summary of the parameters tested during the study of the influence of the AR on immunofluorescence technique results on thick samples. Two different samples were tested during the analysis of the influence of AR on staining's intensity and sensibility. In order to compare results, samples were cut in three and each piece underwent a different parameter.

First, FFPE blocks were deparaffinized in xylene at 37°C for 2 days. Then, samples were incubated in 100% methanol (M1400/15, Fisher Bioreagents™) at room temperature, three times for one hour and another hour at 4°C, followed by an overnight incubation with 66% dicloromethane (DCM) (270997-1L, Sigma)/33% methanol (v/v).

On the next day, samples were washed twice in methanol and incubated overnight in 5% H₂O₂ (H/1750/1, Fisher Bioreagents™,)/100% methanol. Samples were washed in 1x PBS, followed by an incubation in 0.2% PBS-T, twice for 1 hour and then incubated for two days at 37°C, with 20% dimethyl sulfoxide (DMSO) (BP231-1L, Fisher Bioreagents™,)/0.2% PBS-T/0.3M/L glycine (3570-500GM, Calbiochem), to prevent background.

After, only samples with presoaking were incubated in the pH 9 AR solution for 24 hours, at 37°C before the AR step, while the others were kept in 1x PBS. The AR solution was pre-heated for 30 minutes in the steamer at 90°C and AR was then performed for 20 minutes or 40 minutes, accordingly to the defined variables.

For the sample without presoaking, after the glycine incubation, AR was performed as described above. For the sample without AR, this step was omitted.

After, non-specific blocking was made with 0.2% PBS-T/10%DMSO/6% BSA for 2 days at 37°C. Two washes of PBS/0.2% Tween-20® with 10ug/mL heparin (BP2524, Fisher Bioreagents™) (0.2% PBS-Th) were made at 37°C for 1 one hour, right before antibody incubation with anti-CK 19 Alexa Fluor® 568 conjugated antibody (Clone EP1580Y, ab203445, Abcam), diluted 1/400 in 5%DMSO/3%BSA/0.2% PBS-Th for 4 days at 37°C. Washes in 0.2% PBS-Th were made at room temperature.

All steps were done in the shaker (Fisher) with the sample protected from the light.

After the immunofluorescence staining, 50 µm-thick slices were produced using the vibratome (VT1000S, Leica). Samples were embedded on 2.4% agarose (50004, Lonza) and slices were collected sequentially on glass slides.

All sections were microscopically evaluated accordingly to the staining specificity, homogeneity and staining intensity. When heterogeneous, the pattern and range of intensities were explained.

2.3.2 – Application of different incubation time and centrifugal forces on normal 2 mm-thick FFPE blocks

To optimize antibody incubation parameters, three FFPE blocks of normal pancreas, from the same patient, were used. The protocol followed is the same as the one described above, in section 2.3.1, with presoaking for 24 hours and AR for 40 minutes.

Different antibody incubation parameters were used for the incubation with anti-CK 19 Alexa Fluor® 568 conjugated antibody (Clone EP1580Y, ab203445, Abcam), dilution 1/400:

- Incubation for 4 days, no centrifugation, just shaking;
- Incubation for 4 days, 14 hours shaking and 10 hours centrifugation (Thermo Scientific, Sorvall ST 40R) at 600g;
- Incubation for 7 days, no centrifugation, just shaking.

In all parameters, antibody incubation was done at 37°C, protected from light and a reinforcement of antibody, keeping the same dilution, was done on the third day of incubation.

Samples were left in 0.2% PBS-Th with 0.1% of sodium azide (S2002, Sigma), to prevent fungus contamination, until clearing step.

Samples were dehydrated in 70% and 96% methanol, 45 minutes each, followed by two incubations with 100% methanol for 30 minutes and another for 1 hour before incubation in 66% DCM/33% methanol for 3 hours. Then, samples were placed for 15 minutes in DCM before incubation for 2 days in DBE (33630, Sigma).

2.3.3 – Collagenase pretreatment on FFPE blocks with PDAC and a high fibrotic content

Seven FFPE blocks from the same case, previously diagnosed with PDAC and with high desmoplastic content were used.

A similar protocol was used as described above, in section 2.3.2, with an incubation of 7 days for the primary antibody incubation with anti-CK 19 Alexa Fluor® 568 conjugated antibody (Clone EP1580Y, ab203445, Abcam), dilution 1/400. Two different FFPE blocks had the same enzymatic pretreatment, type I collagenase (CLS-4, Worthington, 1mg/mL), type IV collagenase (J13820, Alfa Aesar, 1mg/mL) or both type I and IV collagenase (1mg/mL), on two different set points: before glycine incubation and after blocking step. Each FFPE block was cut in two pieces with similar sizes, to test in each portion, of the same sample, different incubation times: 1 hour and 3 hours.

Experimental groups with the different treatments are summarized in Table 2.

Enzymatic treatment type	Before glycine	After blocking
Type I collagenase	Sample 12	Sample 35
Type IV collagenase	Sample 13	Sample 36
Type I and IV collagenase	Sample 14	Sample 37
Control	Sample 11	Sample 11

Table 2- Summary of the parameters tested during the study of the influence of enzymatic pretreatment on antibody penetration on samples with PDAC. Different enzymatic pretreatment, with type I, type IV or both collagenases in two different time points (for 1 hour and 3 hours) before glycine incubation and after blocking step were tested. Each sample was divided in two, so that one portion had the enzymatic digestion for 1 hour and the other for 3 hours.

For each set point a negative control was run in 1x PBS for 3h. During enzymatic pretreatment samples were placed at 37°C and then transferred to cold PBS, to stop the enzymatic digestion.

2.3.4 – Validation of anti-p53 and anti-AGR2 antibodies on a 2 mm-thick positive control

In order to guarantee that the signal given by anti-p53 and anti-AGR2 antibodies could be detectable, in our samples of interest, two FFPE blocks, one with ovarian serous carcinoma and another with rectal adenocarcinoma were used as positive control for p53 and AGR2, respectively.

For the definition of the positive control for AGR2, three FFPE samples, with rectal adenocarcinoma, were compared with immunofluorescence on 5 µm-thick slices with anti-AGR2 Alexa Fluor® 555 conjugated antibody (Clone EPR3278, ab215293, Abcam), dilution 1/200. Sample with the most intense signal was chosen.

For the definition of the positive control for p53, diagnostic archival slide stained with anti-p53 was used, to verify the presence of a high expression of this protein.

The protocol followed for both samples is the same as described in the section 2.3.2, with an incubation of 7 days for the primary antibody:

- Anti-AGR2 Alexa Fluor® 555 conjugated antibody (Clone EPR3278, ab215293, Abcam), dilution 1/200;

- Anti-p53 Alexa Fluor® 647 conjugated antibody (Clone DO-7, SC47698 AF647, Santa Cruz Biotechnology), dilution 1/50.

2.4 – Multiplex in cleared FFPE blocks of human pancreatic tissue

All five FFPE blocks considered in this study, were processed as described above, in section 2.3.3, with an enzymatic pretreatment with type I collagenase for 1 hour before glycine incubation and 7 days antibody incubation with concomitant:

- Anti-CK 19 Alexa Fluor® 568 conjugated antibody (Clone EP1580Y, ab203445, Abcam), dilution 1/400;
- Anti-AGR2 Alexa Fluor® 488 conjugated antibody (Clone EPR3278, ab215293, Abcam), dilution 1/200.

2.5 – Imaging and data analysis

All 5 µm-thick sections produced during antibodies' optimization and analysis of the influence of AR in the signal intensity and homogenization were evaluated on the Zeiss Axio Imager M2, an upright wide field microscope, equipped with a fluorescence lamp, using a 20x dry objective (Pl-Apochromat). This microscope is equipped with a MRm CCD camera. Filters set were used are summarized in Table 3.

Filterset	Excitation (nm)	Dichroic (nm)	Emission (nm)
DAPI	365	395	445/50
Alexa Fluor® 555 and 568	572/25	590	629/62
Alexa Fluor® 647	640/30	660	690/50

Table 3 - Excitation and emission range in the filterset used for the microscopic evaluation of 5 µm-thick slices. All cleared FFPE blocks were imaged on the Ultramicroscope II, (LaVision BioTec, Bielefeld, Germany), using ECi as imaging solution (Table 4).

Filterset	Laser excitation (nm)	Filter emission (nm)
Alexa Fluor® 488	488	525/40
Alexa Fluor® 555 and 568	561	620/60
Alexa Fluor® 647	640	680/30

Table 4 - Excitation of the laser and filter emission used during imaging acquisition on the Ultramicroscope II (LaVision).

Images acquisition was done with dual side illumination with the following parameters (Table 5):

	Antigen	Zoom	Laser excitation	Laser intensity	Exposure time	NA	SW	Z-stack
CK19Optimization/Validation	CK19 (section 2.3.2)	1x	561	15%	100 ms ⁻¹	0.176	50%	75 μm
	CK19 (section 2.3.3)	0.8X	561	15%	100 ms ⁻¹	0.176	50%	75 μm
	AGR2 (section 2.3.4)	2.5 x	561		50 ms ⁻¹	0.156	30%	12 μm
	P53 (section 2.3.4)	4 x	640	55%	200 ms ⁻¹	0.103	20%	12 μm
	P53 (section 2.3.4)	4 x	561	15%	200 ms ⁻¹	0.103	20%	12 μm
Multiplex	CK 19 (section 2.4)	0.63 x	561	5 %	100 ms ⁻¹	0.156	30%	20 μm
	AGR2 (section 2.4)	0.63 x	488	60%	100 ms ⁻¹	0.156	30%	20 μm

Table 5 - Imaging acquisition parameters for anti-CK 19, anti-AGR2 and anti-P53 antibodies on thick samples. Samples for multiplex were acquired with an overlap of 50% between tiles.

3D reconstruction and analysis were done with Fiji (<https://imagej.net/Fiji>) and Imaris Software x64, version 9.3.1 (Bitplane, Zurich, Switerland).

3. Results and Discussion

3.1 – Definition of antibodies parameters on thin sections

3.1.1 – Definition of CK 7 and CK 19 expression on ductal epithelial cells

Both CK 7 and CK 19 are low molecular weight CKs, present in the intermediate filaments and expressed by epithelial cells. Although present in epithelial cells, loss of CK 7 has been described in poorly differentiated pancreatic ductal adenocarcinomas (1). It was extremely important to choose a consistent epithelial marker, capable of staining normal and altered epithelial cells, such as the one in PanIN and PDAC. This epithelial marker should allow, in a 3D context, the correct phenotypical identification of our population of interest, the pancreatic ductal system.

Three cases, with normal and adenocarcinoma cells were stained and staining's specificity, sensibility and intensity were compared between these two antibodies.

In the normal epithelial cells, no differences were seen in the specificity, sensibility and staining intensity between antibodies (Figure 8).

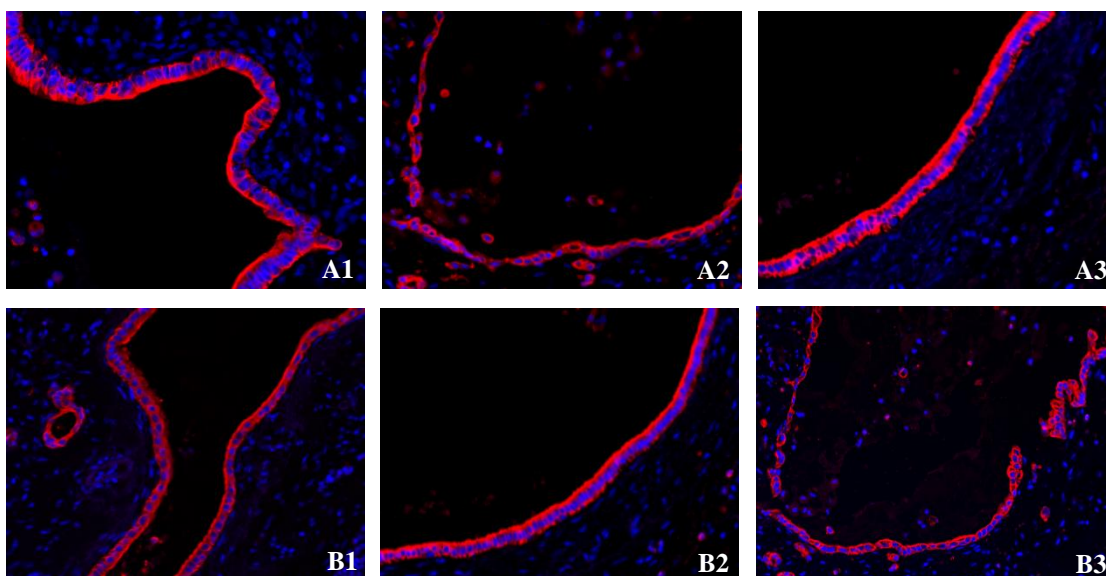


Figure 8 - Anti-CK 7 and anti-CK 19 (AlexaFluor® 594) antibodies expression in normal pancreatic ducts. 5 µm-thick slices of normal pancreatic ducts stained with anti-CK 7 (A1 to A3) and anti-CK 19 (B1 to B3) (red) from three FFPE blocks with PDAC. DAPI was used as nuclear counterstain (blue) (20x).

Also, when observing the results on PDAC cells, similar findings were observed, with high specificity and sensibility in a highly intense signal (Figure 9).

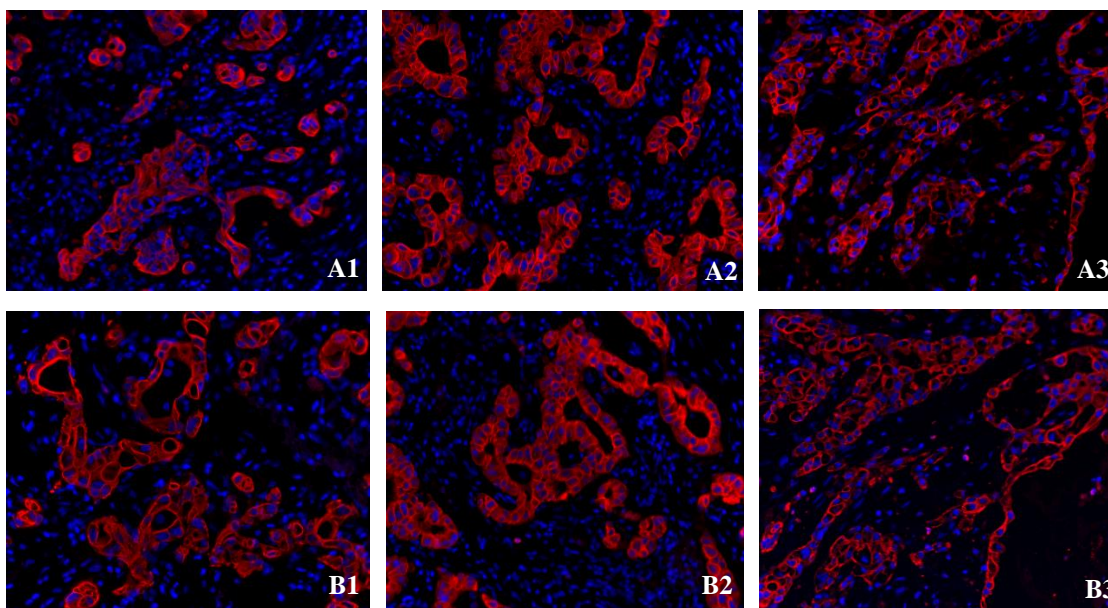


Figure 9 - Anti-CK 7 and anti-CK 19 (AlexaFluor® 594) antibodies expression in PDAC. 5 μ m-thick slices of PDAC cells stained with anti-CK 7 (A1 to A3) and anti-CK 19 (B1 to B3) (red) from three FFPE blocks with PDAC. DAPI was used as nuclear counterstain (blue) (20x).

In the three cases tested, both antibodies presented a strong and specific signal in normal pancreatic ducts and adenocarcinoma cells. Although no differences were observed in these three cases, CK 19 was chosen as epithelial marker since it provided a strong signal and no evidences of its loss in PDAC was found in the literature, as it occurs with CK 7 (1).

3.1.2 – Anti-CK 19 antibody [EP1580Y] (Alexa Fluor® 568), anti-AGR2 antibody [EPR3278] (Alexa Fluor® 555) and anti-p53 antibody [SC53394 AF647] (Alexa Fluor® 647) optimization protocol

For the CK 19 AlexaFluor® 568 conjugated antibody two dilutions were tested, 1/200 and 1/400. In both, no background was observed and specific staining was present in the ductal cells. As shown in Figure 10, both dilutions gave an intense staining, with a saturation of signal detected in the higher concentration. Besides of being specific for pancreatic ducts, this antibody was also able to detect small centroacinar cells, which constitute the beginning of the ductal system, that are in close relationship with the acinar structures.

Considering these results, 1/400 was the dilution chosen, since it presented a specific binding and an intense signal without background.

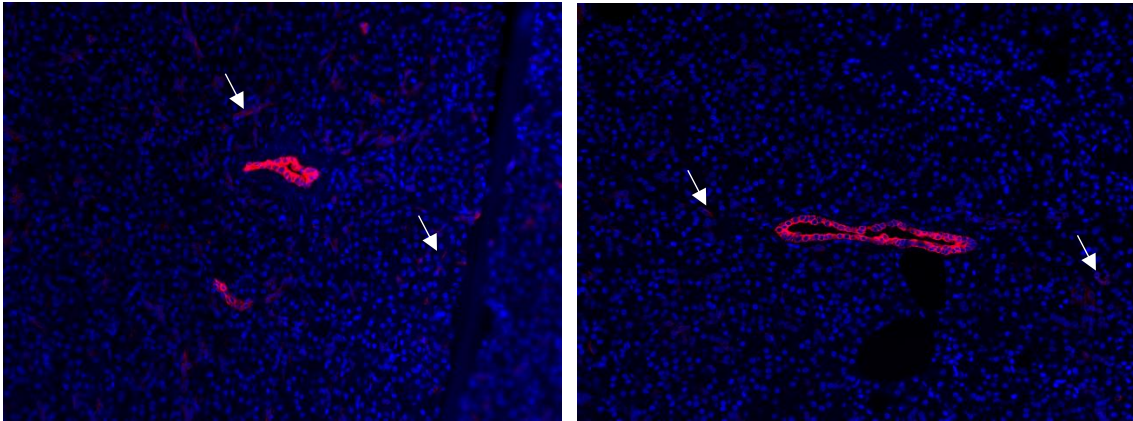


Figure 10 - Anti-CK 19 (AlexaFluor® 568) antibody optimization in normal pancreatic ducts. Normal pancreatic ducts stained with anti-CK 19 antibody (red) with two dilutions, 1/200 and 1/400 (left to right). Arrow indicates the centroacinar cells, identifying the beginning of the ductal system. DAPI was used as nuclear counterstain (blue) (20x).

For the anti-AGR2 AlexaFluor® 555 conjugated antibody, three different dilutions were tested: 1/50, 1/100 and 1/200.

In adenocarcinoma cells a specific and intense staining without background or non-specific staining was observed. With the higher dilution, there's a signal saturation and with the lower dilution a small decrease in intensity is observed (Figure 11), still considered highly intense. With this evidence, 1/200 was considered the best dilution for anti-AGR2 antibody, assuring the best performance, without loss of signal nor expense of unnecessary resource.

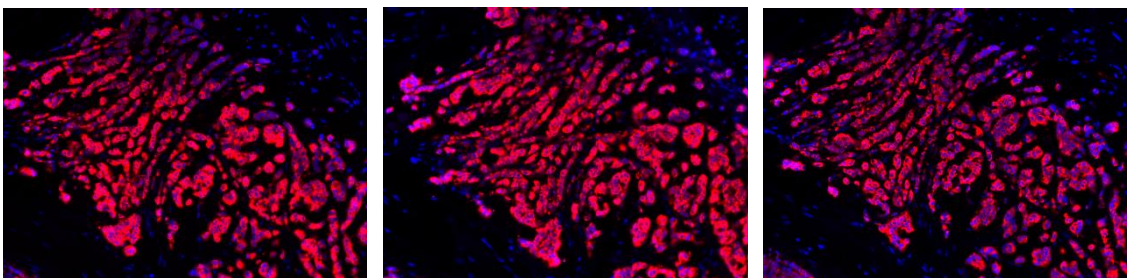


Figure 11 - Anti-AGR2 (AlexaFluor® 555) antibody optimization in rectal adenocarcinoma. Rectal adenocarcinoma stained with anti-AGR2 antibody (red) with dilutions 1/50, 1/100 and 1/200 (left to right). Rectal adenocarcinoma cells positive for AGR2. DAPI was used as nuclear counterstain (blue) (20x).

For the anti-p53 AlexaFluor® 647 conjugated antibody three different dilutions were tested, 1/50, 1/100 and 1/200.

This antibody showed a weak signal, only detectable with long exposure time during imaging acquisition, for all the dilutions tested. As shown in Figure 12, only nuclear staining was observed in carcinoma cells, which was specific.

Before the usage of the anti-p53 antibody from Santa Cruz Biotechnology, we tested two other antibodies - anti-p53 Alexa Fluor® 647 conjugated antibody (Clone E26, ab224942, Abcam and clone DO2, SC53394 AF647, Santa Cruz Biotechnology) - but these presented weaker signal and lower specificity, with the presence of some cytoplasmic pattern (data not shown).

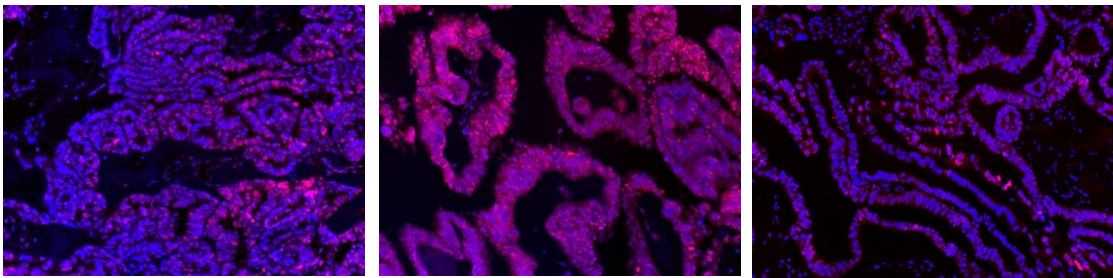


Figure 12 - Anti-p53 (AlexaFluor® 647) antibody optimization in lung squamous cell carcinoma. Squamous cell carcinoma stained with anti-p53 antibody (red) with dilution 1/50, 1/100 and 1/200 (left to right). Nuclear pattern is seen with anti-p53 that co-localizes with DAPI, used as nuclear counterstain (blue) (20x).

All dilutions presented specific staining and similar results, with a mild non-expected cytoplasmic staining, although when using 1/200 a signal reduction could be noticed. Dilution 1/100 was considered the correct one, since it could give a specific staining without compromising the signal nor causing unnecessary expenses of antibody.

3.2 – Influence of AR, enzymatic pretreatment and antibody incubation parameters on thick samples

3.2.1 – AR for 40 minutes after presoaking increases signal-to-noise ratio

The two FFPE blocks used in this experiment were divided in three smaller fragments, to test on the same sample, three different conditions: no AR, AR without presoaking and AR with presoaking. Besides, two different AR incubation times were tested, in this case 40 minutes for sample 4 and 20 minutes for sample 5, to see which condition could give the most homogenous and efficient staining signal.

AR is an essential step in immunohistochemistry on slices, since it reverses the conformational modifications induced by the fixative, being formalin the most commonly used. Fixation with formalin is an essential step to preserve samples and stabilize cellular content, avoiding putrefaction and autolysis. It reacts with amine groups and cross-links with the tissue and its components, which causes a conformational alteration of proteins, that can decrease their recognition by the antibodies, potentially leading to false negatives (66).

To reverse these conformational modifications, enzymatic digestion or heat-induced epitope retrieval, with different pH, can be applied. In this case, we tested heat-induced epitope retrieval with pH9 for CK 19 since it was the condition that worked better for our antigen of interest in 5 μm -thick sections.

As shown in Table 6, thickness of tested samples ranged from 700 μm to 1550 μm . Specific staining was detected in every section and in all intensity ranged from high to low.

	Sample 4			Sample 5		
	Standard	AR 40 min (No presoaking)	AR 40 min (Presoaking)	Standard	AR 20 min (No presoaking)	AR 20 min (Presoaking)
Slices (N)	28	31	25	25 ¹	21	14
Specific staining	100%	100%	100%	100%	100%	100%
Staining homogeneity	7,1%	0%	12%	28% (7)	38.1%	14.3%
Heterogeneity pattern	Periphery more intense than center	Periphery more intense than center	Random/sideways/periphery more intense than center	Periphery more intense than center	Periphery more intense than center	Random/sideways/periphery more intense than center
Intensity	H-L	H-L	H-L	H-L	H-L	H-L
Size	1 x 0.7 cm	1 x 0.6 cm	1 x 0.5 cm	0.6 x 0.6 cm	1 x 0.6 cm	1 x 0.5 cm
Thickness	1450 μm	1550 μm	1250 μm	1250 μm	1050 μm	700 μm

Table 6 - Summary results of the microscopic observation of two FFPE blocks of normal pancreas (sample 4 and 5) with three different conditions: standard protocol without AR, AR for 40 or 20 minutes with and without presoaking in the AR solution. Presence of specific staining, staining homogeneity and intensity range was evaluated. Staining intensity was classified as high (H), medium (M) or low (L). (1) Presence of air bubbles invalidated the analysis of the first section.

Most sections presented a heterogeneous staining pattern, mainly more intense in the periphery than in the center, which represents the passive diffusion of the antibodies,

meaning that the edges of the sample are the first to contact with the antibodies and those antigens are the first to bind to the antibodies (Figures 13 and 14). The inner antigens, although present, bind to a much limited amount of antibodies, due to the difficulty that they have to penetrate deep in the tissue, that is composed by a tight mesh of biological molecules. In a small portion, a homogeneous staining was detected but, it was only visible when the section evaluated corresponded to a small and limited portion of the tissue.

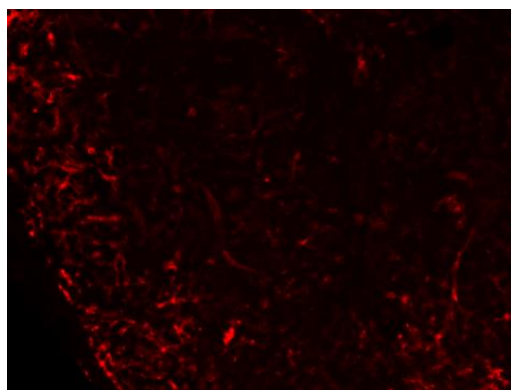


Figure 13 - Heterogeneous staining pattern of a representative section with anti-CK 19 (AlexaFluor® 568) antibody. Sample 5, with AR for 20 minutes without presoaking, shows in the periphery a higher staining intensity of anti-CK 19 antibody (red) that decreases as it progresses to the center of the slice (20x).

When comparing the pictures shown in Figure 14, a lower signal-to-noise ratio is achieved in the protocol that did not perform AR. When this step is added, staining signal increases, making it more obvious when compared to the background. This is especially notable in sample with AR after presoaking in the AR solution for 24 hours. As for all the reagents, AR solution diffuses passively in the tissue which requires time, especially in thick samples.

As mentioned above, AR reverses the conformational changes of proteins made by the fixation step, making it detectable again. This increase of signal in the samples with AR can be explained by this phenomenon. Antigens present in the tissue could not be detected by the antibody in the samples without AR, due to the conformational alteration during fixation, which lowers the amount of structures detected, increases staining's heterogeneity and decreases signal's intensity. With the application of AR, for 40 minutes and 20 minutes, an increase of signal was observed, with a higher signal-to-noise ratio and more structures detected.

In both samples, the best result was achieved with presoaking on AR solution and although a difference in the signal intensity was not noticed, sample that had AR for 40 minutes after presoaking, detected more specific structures than the one that had AR for 20 minutes, which helped reducing staining heterogeneity.

The application of this procedure has already been published in some papers (56,71). First, Lui *et al.* (2017) developed FASTClear that combined iDISCO with CLARITY, and its SDS delipidation to clear and immunostain human brain tissue. Here, SDS, besides of acting as a delipidation agent, also acts as a protein denaturant, which will be responsible for the AR effect. Then, the importance of AR was also brought by Saritas *et al.* (2018), who performed AR with citrate buffer for 1 hour on 1 to 2 mm-thick sections of kidney, analyzing the tubule remodeling in adult mouse kidneys, cleared with ECI. Both papers, although revealing the importance of AR, didn't compare staining intensity and homogenization between samples without and with AR. Besides, none of them suggested the incubation of the sample in the AR solution before the AR step itself, which with our results, show evidences that it's crucial to increase the amount of positive structures detected.

Nevertheless, a homogenous pattern was not completely achieved with any of the conditions tested, which could be explained by the absence of sufficient amount of antibody or insufficient incubation time, that didn't allow an even distribution of reagent throughout the sample. In order to test this, two other trials were done, one in which a supplement of antibody was added during antibody incubation and another trial where the antibody incubation was longer or although with the same duration, centrifugal forces were applied to promote antibody penetration (section 3.2.2).

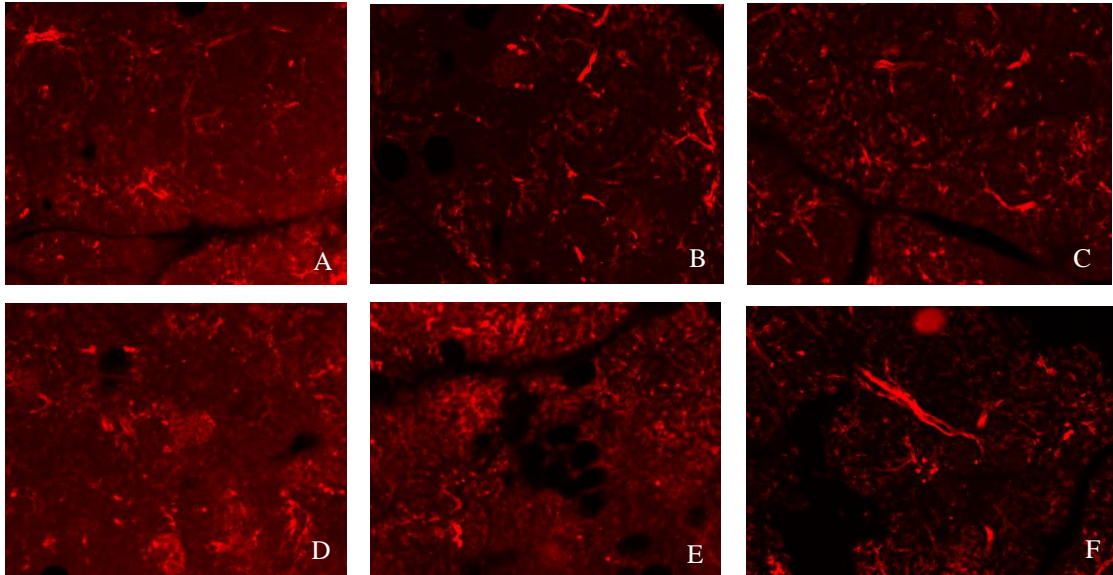


Figure 14 – Influence of AR on thick samples from FFPE blocks of normal pancreas. First row: Sample 4: A - no AR, B - AR for 40 minutes without presoaking, C - AR for 40 minutes after presoaking in the AR solution for 24h at 37°C. Second row: Sample 5: D - no AR, E - AR for 20 minutes without presoaking, F - AR for 20 minutes after presoaking in the AR solution for 24h at 37°C. Samples were stained with anti-CK 19 (AlexaFluor®568) antibody (red). A higher signal-to-noise ratio is seen in the protocol with AR after presoaking, when compared to the standard and the AR without presoaking protocols. Sample 4, that had longer AR, presents better signal-to-noise and more evidence of positive structures (20x).

Although for this experiment, due to the absence of the ultramicroscope, the analysis was made with 50 μm -thick slices, which limited the 3D perception of the real penetration and homogeneity of the staining, it was still possible to see the complex relationship between all the ductal components and its tridimensionality, as shown in Figure 15, with the observation of the beginning of the ductal system with centroacinar cells, that are in close relationship with acini cells, joining the intercalated ducts.

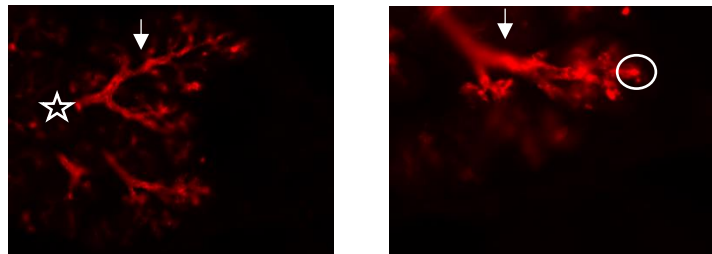


Figure 15 - Ductal system organization. Centroacinar cells (right, circle), stained with anti-CK 19 (AlexaFluor® 568) antibody (red), joining intercalated ducts (right and left, arrow) that will converge into intralobular ducts (left, star) in pancreas 4 with standard protocol (magnification 20x and 40x, left to right).

3.2.2 – Longer antibody incubation favors staining’s homogeneity and intensity

Incubation times and parameters were tested in three FFPE entire blocks of normal pancreas. Besides of extending the incubation from 4 days to 7 days, the application of centrifugal forces was also explored to see if it could speed the process and increase the penetration.

These were the first samples analyzed under the ultramicroscope. The clearing protocol chosen was an organic solvent-based protocol, since we would be dealing with fibrotic samples in the future. DBE was used as the RI matching solution, which, since it has a high RI, was expected to have a fast and good clearing ability (53).

All samples were cleared correctly after two days in DBE (Figure 16). Sample’s consistency was harder after clearing, which was also expected since the sample losses its water content, after dehydration in methanol, which reduces its flexibility and hardens its consistency. Although cleared with DBE, samples were imaged with ECi to reduce the personal exposure to hazard reagent (Appendix 1). Both solutions have a high RI that didn’t reduce the imaging ability.

The presence of Indian ink, used for anatomical references during the macroscopic exam for diagnosis purposes, compromised the light penetration and caused some unwanted scattering and absorption, but in this case, it did not limit the ability of visualizing specific signal.

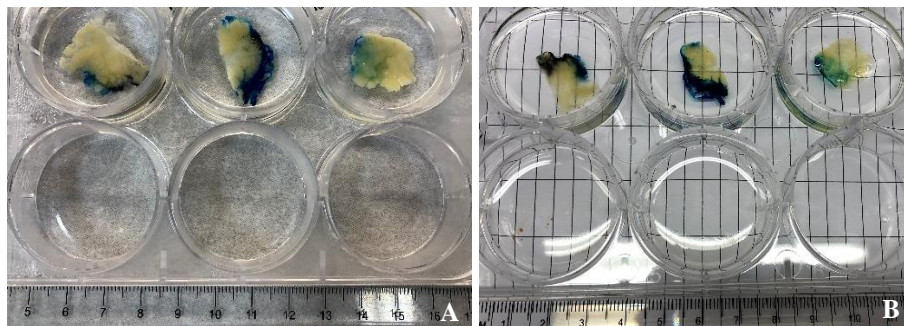


Figure 16 - Clearing efficiency with DBE. Three FFPE blocks with normal pancreas (sample 8, 9 and 10 from left to right) before (A) and after (B) clearing. After clearing it's possible to see through the sample, identifying the lines under it.

When analyzing the results, a more homogeneous antibody distribution is seen in the sample that was incubated in the antibody for seven days. In this sample, it is possible to clearly see the ductal system, its distribution and connections between different ducts.

In the samples that were incubated for shorter time (4 days with or without centrifugation), although positive staining was present, this was more granular and sparse, which indicates that the antibody needs to be in contact with the tissue for at least 7 days in order to reach to all its areas and bind to antigens (Figure 17).

Centrifugation leads to the sedimentation of components, forcing the penetration of antibodies into the tissue. Although better than the control sample, since it showed more ductal paths, sample with 4 days and centrifugation wasn't as effective as the sample with passive diffusion for 7 days.

The application of physical forces was already used by other authors (50,54,69). For instance, Lee *et al.* (2016) compared antibody penetration with centrifugation and pressure. Sample with passive diffusion achieved a penetration of 30-100 μm after an incubation of 1 to 2 days, but only around 3 hours were needed to achieve the same penetration depth with the application of pressure or centrifugal forces (50). Also, in vDISCO, pressure is applied to increase the penetration of nanobodies and the permeabilization solution (54).

Although in the Nöe *et al.* (2018) report they achieve a penetration in normal pancreatic tissue of 0.7 to 1.5 mm with the increase of antibody supply and rounds of centrifugation (69), with the similar parameters to the ones tested here, our results show that passive diffusion is more effective than a shorter incubation with centrifugal forces.

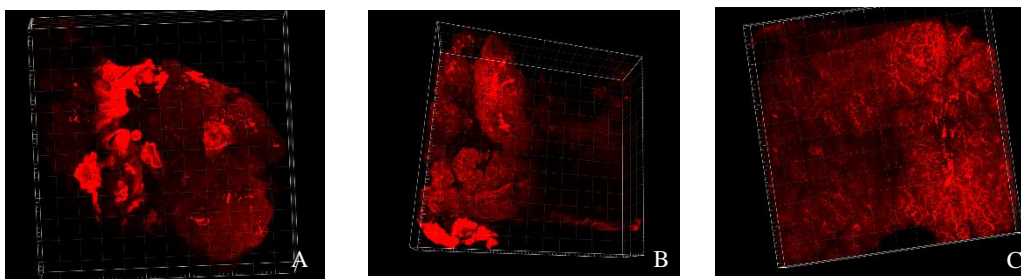


Figure 17 - 3D picture from three FFPE blocks of normal pancreas with anti-CK 19 (AlexaFluor® 568) antibody. Samples were stained with anti-CK 19 (AlexaFluor® 568) antibody (red), which revealed the epithelial component, the ductal system. A – Antibody incubation for 4 days (sample 9, control sample). B – Antibody incubation for 4 days, 14h shaking and 10h centrifugation at 600g (sample 8). C – Antibody incubation for 7 days (sample 10) (1x).

We hypothesize that besides of the physical forces that could help in the penetration, the major and more important aspect to achieve a full and homogeneous penetration is the availability of antibody, especially in large samples.

In this protocol, a second supply of antibody was done on the third day to see if it could decrease staining heterogeneity. Before applying in these three samples, a test was done on a FFPE block with normal pancreas (sample 6), with anti-CK 19 AlexaFluor® 568 conjugated antibody (dilution 1/400) for 4 days with a supplement of antibody on the third day, keeping the same concentration of antibody. In this sample the staining differences between the periphery and the central portion of the slice was not so clear and a high number of positive structures were detected (Figure 18).

This evidence points that the amount of antibody for large and thick samples has to be reinforced to guarantee its availability for all the antigens present in the tissue, especially if it's a tissue with a high quantity of those proteins, as happens with these samples. This evidence is in agreement with some results already published (56,68,69,73).

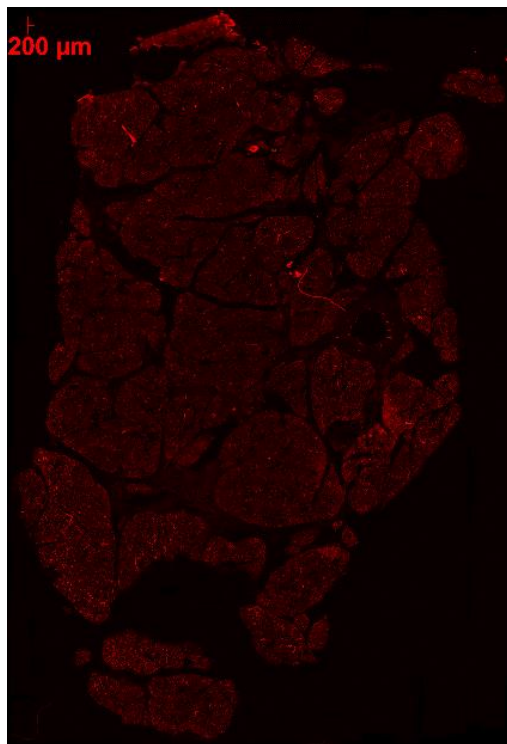


Figure 18 – Antibody supply experiment on an entire FFPE block of normal pancreas. Mosaic picture of the 10th slice of sample 6 with a reinforcement of anti-CK 19 (AlexaFluor® 568) antibody (red, 10x).

3.2.3 – Type I collagenase digestion promotes antibody penetration on PDAC thick samples

Seven FFPE blocks from the same case, previously diagnosed with PDAC and with a high desmoplastic content were used in order to infer if an enzymatic pretreatment could lead to a more homogeneous and deeper antibody penetration, through the degradation of the collagen present, type-I collagen in the interstitial space and type-IV collagen surrounding cancer cells (8).

PDAC, as mentioned before, is characterized by a high ECM content that constitutes a physical barrier to the penetration of antibodies (50). For instance, Nöe *et al.* (2018) only achieved a penetration with non-conjugated antibody anti-CK 19 of 0.3 mm to 0.6 mm in FFPE of human cases with PDAC, compared to 0.7 mm to 1.5 mm in normal pancreatic blocks (69).

These results are caused by the barrier that high fibrotic content, characteristic of PDAC, form against antibody penetration. Öhlund *et al.* (2013) studied the collagen content in PDAC and showed that type I collagen was highly expressed in the desmoplastic area, being produced by pancreatic stellate cells, but type IV collagen, produced by pancreatic cells, deposits around them forming a basement like structure (8).

Although type I collagen is more abundant, we sought to understand if the reduction or complete removal of type I, IV or both, for two different time points, would increase antibody penetration in PDAC, reducing the efficiency difference of deep antibody immunolabelling between a normal pancreas and PDAC, without compromising its normal architecture.

All blocks came from the same patient and the same block was used to test different incubation times, 1 hour and 3 hours, in order to reduce the variability between samples and guarantee a viable comparison.

Besides of the staining intensity and penetration, general morphology was evaluated. Samples that had enzymatic pretreatment before glycine conserved their elastic consistency. On the other hand, samples with enzymatic pretreatment after blocking, suffered a consistency alteration, presenting a mucoid consistency. They had to be

handled with ultimate care since would easily crumble when handled. After clearing, although harder, as expected due to the dehydration, these samples remained fragile and crumbled during the placement on the imaging stage (Figure 19).

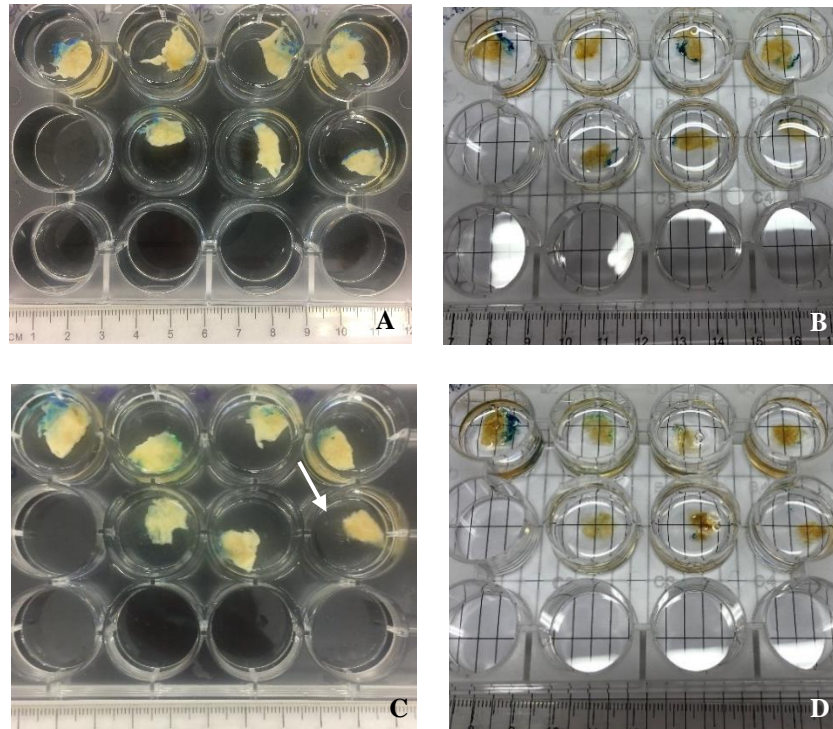


Figure 19 - Enzymatic pretreatment of seven FFPE blocks from the same patient with type I, type IV and type I + type IV collagenase, for 1 hour and 3 hours. A and B – Samples that had the enzymatic pretreatment before glycine. A – Normal macroscopic aspect after enzymatic pretreatment. B – Macroscopic aspect after clearing. C and D – Samples that had the enzymatic pretreatment after blocking. C– Macroscopic aspect after enzymatic pretreatment with a mucoid consistency and a dirty solution (arrow) due to loss of integrity. D – Macroscopic aspect after clearing.

Microscopically, signal intensity and morphology were evaluated. When comparing samples that underwent enzymatic pretreatment before glycine with control samples, an increase of intensity was noticed in all conditions, without significant differences between samples (Figure 20 and Appendix 2).

Also, between different incubation times no significant differences were seen in the intensity nor in the general morphology, with the exception of the sample that had the combination of enzymes for longer, where a diminution of the cancer cells cluster contour was noticed. This alteration was expected since a combination of enzymes for 3 hours is much more aggressive to the tissue than a shorter incubation with only one enzyme.

When analyzing the results from the samples processed with enzymatic digestion after blocking, the same increase of staining was noticed, compared with the control, with exception of the sample with both enzymes (Figure 20 and Appendix 2). Besides of this alteration, a decrease of the general morphology was visible, both macroscopically and microscopically, with a much fainter cellular contour.

Only sample digested for 1 hour with type IV collagenase after blocking didn't present any type of signal. This absence was due a wrong sample selection, since this portion didn't have any pancreatic component, when analyzing the HE slide (Appendix 2).

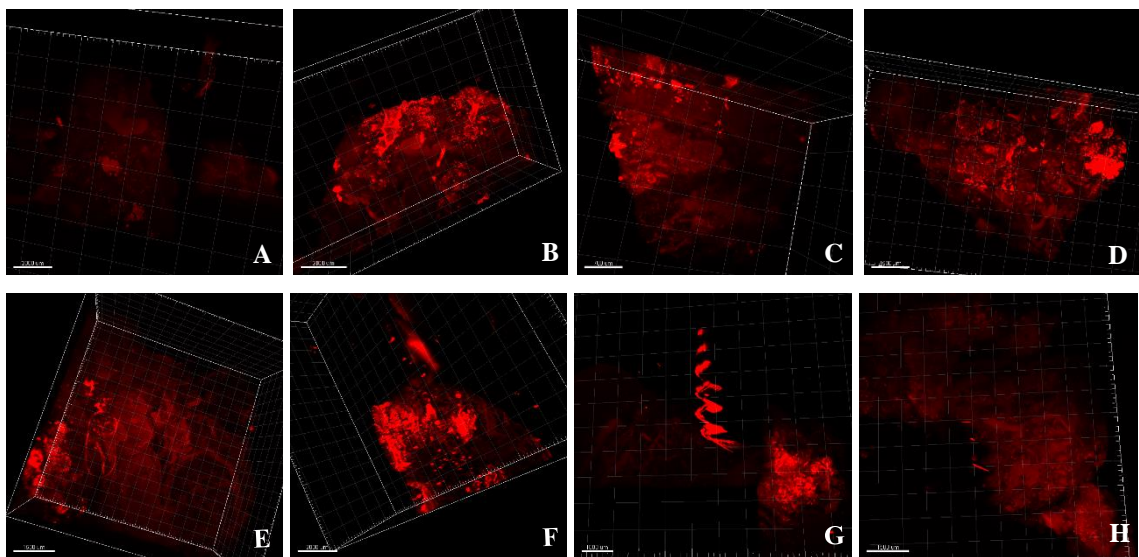


Figure 20 - 3D aspects of the control sample and samples processed before glycine and after blocking for 3 hours with type I and IV collagenase. Samples were stained with anti-CK 19 (AlexaFluor® 568) antibody (red), which revealed the ductal system. A and E – Control sample. B and F – Samples digested with type I collagenase before glycine and after blocking, respectively. C and G – Samples digested with type IV collagenase before glycine and after blocking, respectively. D and H – Samples digested with type I and IV collagenase before glycine and after blocking, respectively. Enzymatic digestion increases staining intensity, especially in the samples processed before glycine. Samples digested after blocking presented a more granular aspect (F) due to the morphological digestion. In image G and H no increase in staining intensity is seen due to the morphological degradation caused by the enzymatic digestion on a physically fragile tissue.

Between all enzymatic pretreatments tested, type I collagenase was the less aggressive to the tissue. Type I collagen is found in the interstitial space, only constituted by fibroblasts and high collagen content. Type IV is found surrounding the cancer cells clusters, resembling a basement membrane. The application of a specific enzyme against this basement-like structure seems to cause some instability and loss of the glandular pattern, normally detected in the cancer clusters.

As discussed before, no differences were seen between the two incubation times with type I collagenase so we considered pretreatment for 1 hour the best approach, since its extension didn't lead to an increase of staining intensity nor antibody penetration, without any benefit to an already long and complex protocol.

From our literature review, this is the first time that this enzymatic approach is used. In vDISCO a similar idea is explored with the usage of trans-1-acetyl-4-hydroxy-L-proline, to loosen the collagen content on an entire mouse (54). Based on the results presented in this study, enzymatic pretreatment can constitute an important step to increase antibody penetration, which will amplify the staining signal since it reduces the physical barrier promoted by the fibrotic content.

Other alternatives or combinations, like the application of a denaturant agent such as urea or N-methylglucamine to remove the collagen content should also be tested in the future to see if it could improve the signal without compromising tissue's integrity or antigenicity (72).

3.2.4 – Anti-p53 and anti-AGR2 staining on thick positive control specimens

For the validation of AGR2, we first sought to choose a sample with high expression of this protein, through immunohistochemistry. In order to do that, three different cases, diagnosed with rectal adenocarcinoma, were stained and compared.

All cases presented specific staining, but the intensity was different between samples. The sample with the highest staining intensity was selected for the validation of this marker on thick samples (Figure 21).

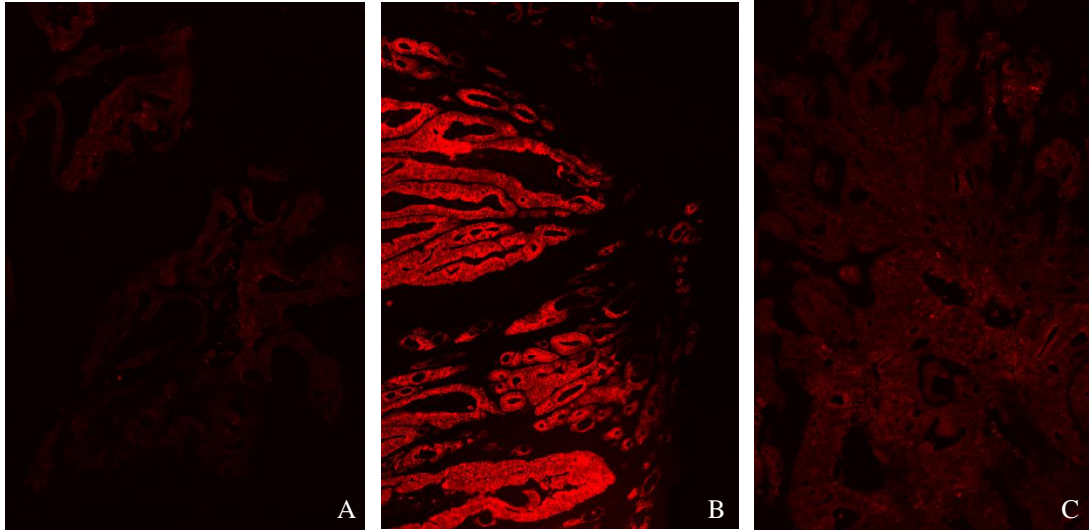


Figure 21 - AGR2 expression in three cases of rectal adenocarcinoma. Samples were stained with anti-AGR2 (AlexaFluor® 555) antibody (red). Staining intensity and extension were evaluated. Sample B presented the highest intensity of AGR2 expression of all three cases (20x).

Sample clearing was very effective, with a high transparency achieved, as shown in Figure 22. Although successfully cleared, an alteration of normal shape was verified, resulting in a bended sample, which influenced negatively the ability to focus it during the 3D imaging. Below the mucosa and submucosa layers, there is the muscular layer that can retract during dehydration, potentially explaining the shape alteration in this case. With the purpose of getting an even focus plan, sample was cut in two before acquisition.

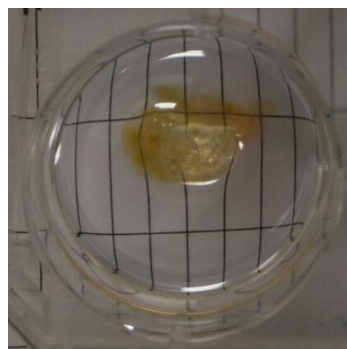


Figure 22 - Human sample with rectal adenocarcinoma after clearing with DBE. Lines under the sample are easily visible after an effective clearing but some morphological alteration is seen due to a bended sample.

Similar to what was observed in the 5 μm -thick slice, a very bright and specific signal in the glandular cells was observed, validating the application and usability of this antibody in thick samples (Figure 23).

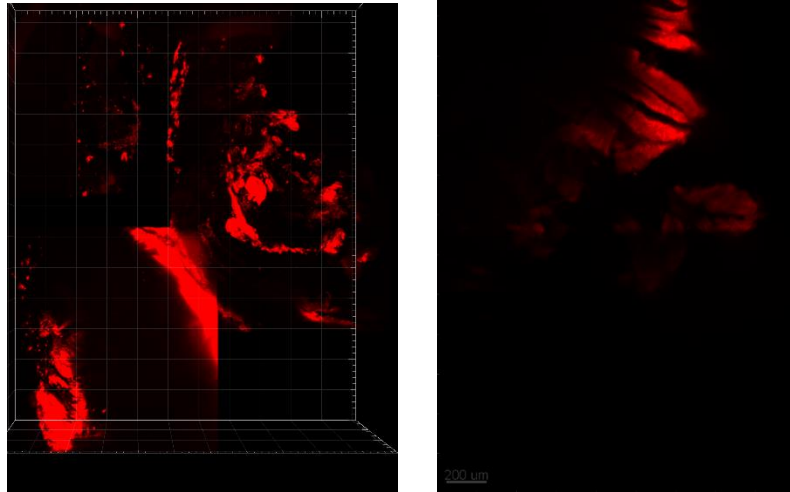


Figure 23 - Anti-AGR2 expression on a thick sample with rectal adenocarcinoma. Sample 40 was stained with anti-AGR2 (AlexaFluor® 555) antibody (red), presenting a specific and intense signal in the glandular component. 3D and 2D perspectives (left-right) (2.5x).

For p53 validation in thick specimens, a high-grade serous carcinoma sample was used, which was also successfully cleared, without significant shape alteration (Figure 24). Nevertheless, due to large sample size it was cut in two before image acquisition.

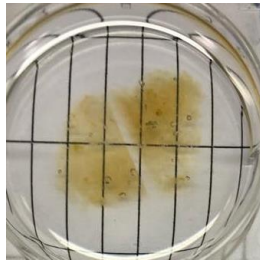


Figure 24 - Human sample with ovarian serous carcinoma after clearing with DBE. Lines under the sample are easily visible, which represents a very good clearing. No morphology alteration is seen.

During image analysis, a very high background was seen in this sample, with different excitation fields and no presence of specific signal was identified.

Nevertheless, although very weak, in some areas, it was possible to distinguish small clusters of round structures, one close to each other, measuring from 17 to 30 μm , that resemble in shape, organization and size the cancer cells' nuclei, seen in the thin section of the positive case (Figure 25).

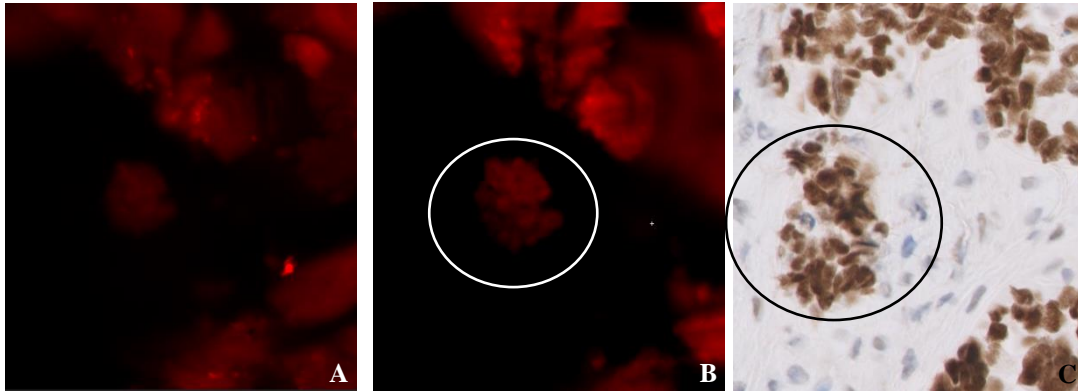


Figure 25- Anti-P53 expression on a thick sample with serous carcinoma. **A and B** - Sample 43 was stained with anti-p53 (AlexaFluor®647) antibody (red). Two different laser excitations were used (A - 561 nm and B - 640 nm). In the picture B a small cluster of round shape structures is seen that resembles nuclei present in the 5 μm -section (white circle). **C** - Chromogenic immunostaining of anti-p53 on the 5 μm -thick section of the same sample, where a cluster of cancer cells is seen, with enlarged nuclei (black circle) (A and B – magnification 4x, C – 40x).

The absence of p53 in this positive sample could be explained by the poor cellular-resolution of the ultramicroscope (68,74,75). An ultramicroscope constitutes a light-sheet microscope that uses illumination perpendicular to the detection system, forming single-plane illumination (light sheet) for optical sectioning. Through the light sheet illumination plane it diminishes excitation of the fluorophores from the lower and above layers, reducing background and lowering photobleaching and phototoxicity (74,75). Acquisition on a confocal microscope, within a custom-made chamber, would increase the resolution of the system, potentially allowing to see nuclear pattern, although it would increase exponentially the acquisition time, besides of causing severe photobleaching (68).

Besides, there's also a physical challenge that nuclear antibodies face compared to cytoplasmic/membrane antibodies, the nuclear membrane. Nuclear antibodies need to penetrate two membrane hydrophobic layers, cytoplasmatic and nuclear, before achieving the target. A better permeabilization may be needed in this case or the usage of smaller antibodies, such as cleaved antibodies or nanobodies. Nanobodies, present in camelids, are single variable domain antibodies, constituted exclusively by heavy chains, with 12–30 kDa in opposition to the 150 kDa of the regular antibodies (76).

Cai *et al.* (2018) used nanobodies conjugated to Atto dyes to enhance the endogenous signal, increasing the signal-to-noise ratio (54). Atto dyes have longer lifetimes and bigger photostability compared to AlexaFluor®, so their application for weaker signals, could lead to better results.

P53 expression, even on thin slices, was always weak, only detectable after long exposure times. We decided to use conjugated antibodies, since it would diminish the protocol time, avoiding the application of secondary antibody, that had to penetrate in a tight mesh of cells, molecules and other antibodies, and eliminating the possible crosstalk between secondary antibodies. Nevertheless, the amplification power gain from a direct immunolabelling method is lower than an indirect method, and for this protein using secondary antibodies could be an essential step to increase the staining intensity.

3.3 – Multiplex studies in cleared FFPE blocks with PDAC

3.3.1 – Histological grade and p53 expression

Before the multiplex analysis and clearing of the samples, p53 expression was assessed through immunohistochemistry in all the cases, since it is described that it is present in 50-75% of the cases of PDAC (27,77).

Table 7 summarizes the histological classification, tumour location, stage and p53 expression of the five samples used for the multiplex staining.

Sample identification	Histological classification	P53 expression	Patient sex	Patient age	Tumor location	Stage
Sample 16	PDAC + PanIN	Positive	Female	77	Head	pT2pN1
Sample 19	PDAC + PanIN	Positive	Male	81	Tail	pT1cpN0
Sample 21	PDAC + PanIN	Negative	Male	75	Tail	pT2pN0
Sample 23	PDAC + PanIN	Negative	Male	60	Head	pT2pN0
Sample 25	PDAC + PanIN	Positive	Female	65	Head	ypT2ypN1

Table 7 - Histological grade, p53 expression, location and staging in the 3D analyzed samples.

Three of the five samples presented P53 expression, which corresponds to 60% of the cases, percentage that is in concordance with the literature review (77). Additionally, patient's age was 60 years old and above, three of them were males and pancreatic head was the most common location, data that is in concordance with the literature (78).

3.3.2. – Multiplex on 2 mm-thick samples

A multiplex staining was planned with three different markers:

- Anti-CK 19 Alexa Fluor® 568 conjugated antibody (clone EP1580Y, ab203445, Abcam), which would identify all the ductal cells;
- Anti-AGR2 Alexa Fluor® 555 conjugated antibody (clone EPR3278, ab215293, Abcam), that would mark PanIN and PDAC, but not the normal ductal cells, being the one responsible for the distinction between normal and abnormal;
- Anti-p53 Alexa Fluor® 647 conjugated antibody (clone DO-2, SC53394 AF647, Santa Cruz Biotechnology), that would phenotypically distinguish high grade PanIN and PDAC from the remaining ductal components.

All of these were conjugated antibodies since, as pointed before, it would reduce the penetration challenge, with just one antibody per marker, decreasing in parallel the cross reactivity and unspecific staining potentially given by the secondary antibodies' crosstalk.

All wavelengths for the conjugated antibodies were chosen in the red and far red spectrum, since it's the one that presents lower background, lower scattering and better penetration (53,54,68). Unfortunately, the filtersets on the ultramicroscope don't distinguish the signal between AlexaFluor® 555 (AGR2) and AlexaFluor® 568 (CK 19), which led to the exchange of anti-AGR2 AlexaFluor® 555 for anti-AGR2 AlexaFluor® 488 antibody (clone EPR3278, ab199044, abcam). Before its application on thick samples, an optimization of the antibody in 5 µm-thick sections was done comparing two dilutions: 1/100 and 1/200 (Figure 26).

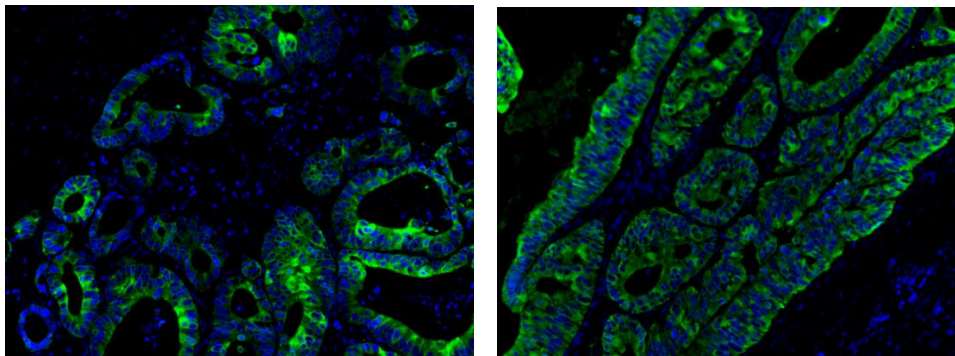


Figure 26 - Anti-AGR2 (AlexaFluor® 488) antibody optimization in rectal adenocarcinoma. Rectal adenocarcinoma stained with anti-AGR2 (green) with dilution 1/100 and 1/200 (left to right). Rectal adenocarcinoma cells positive for AGR2. DAPI was used as nuclear counters (20x).

As happened with the AlexaFluor® 555-conjugated antibody, both dilutions gave specific and intense signal. Although a small reduction in intensity was seen with the highest dilution, the signal is still considered high, so 1/200 was the dilution used for the final samples.

Since anti-p53 didn't worked in our validation samples this marker as not applied in our samples.

For the five processed samples, no alteration of the consistency was seen after the protocol, especially after the enzymatic pretreatment, but a small retraction was seen after AR, mainly on sample 21, on the area with adipose tissue (Figure 27).

All samples were effectively cleared, but due to samples' size some difficulties were encountered during image acquisition, particularly with sample 19 and 23. For this samples, a custom-made sample holder was developed, where the samples were glued with superglue. In these large samples the focusing plane was very hard to get, potentially related with the presence of glue that caused some artifacts.

Additionally, all acquisitions were made with the lowest magnification, 0.63x, due to a malfunctioning on tiles' overlap during images acquisition, which prevented an analysis with higher magnification, that would benefit this analysis.

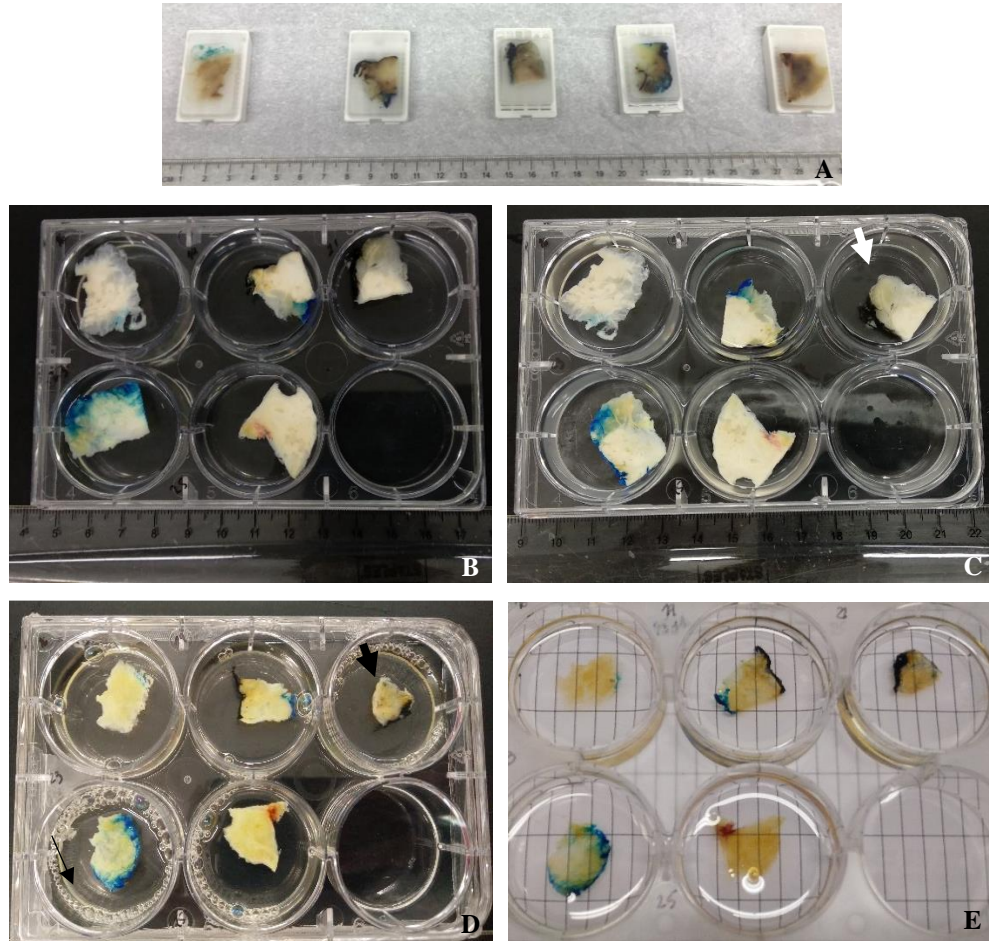


Figure 27 - Macroscopic aspect of the five final samples throughout the protocol. A – Five FFPE blocks. Sample 16, 19, 21, 23 and 25 (from left to right). B – Deparaffinized samples before enzymatic pretreatment. C – Deparaffinized samples after enzymatic pretreatment. No alteration in consistency is observed. D – Deparaffinized samples, after 40 min in the pH9 AR solution. Some retraction is seen, especially in the areas of adipose tissue (arrow). E – Cleared samples in DBE.

In all samples, CK 19 expression was seen, with the most intense signal detected on the periphery of the sample (Figure 28). Nevertheless, positive staining was observed throughout the entire sample, with different intensities. This difference in intensities can be due to the passive penetration rate of the antibodies that connect and bind first to the outer antigens, present in the periphery. Besides, sample 21, the smaller sample, presented the lowest staining heterogeneity, which could point to an insufficient antibody-antigen ratio for these big samples. Although we have compared the results between one and two supplies of antibody, these trials were made in normal pancreas and not in PDAC, which may have higher antigen content.

Anti-AGR2 signal was weaker than anti-CK 19, being mainly present in the periphery of tissues (Figure 28). This antibody was conjugated with AlexaFluor® 488, a

fluorophore with shorter wavelength than AlexaFluor® 568, meaning that it suffers more scattering and cannot penetrate so deep in the tissue, potentially explaining the loss of AGR2 signal observed. Additionally, the green spectrum is characterized as having a higher background, which can diminish the signal-to-noise ratio decreasing the contrast and perception of AGR2 expression with a dim signal.

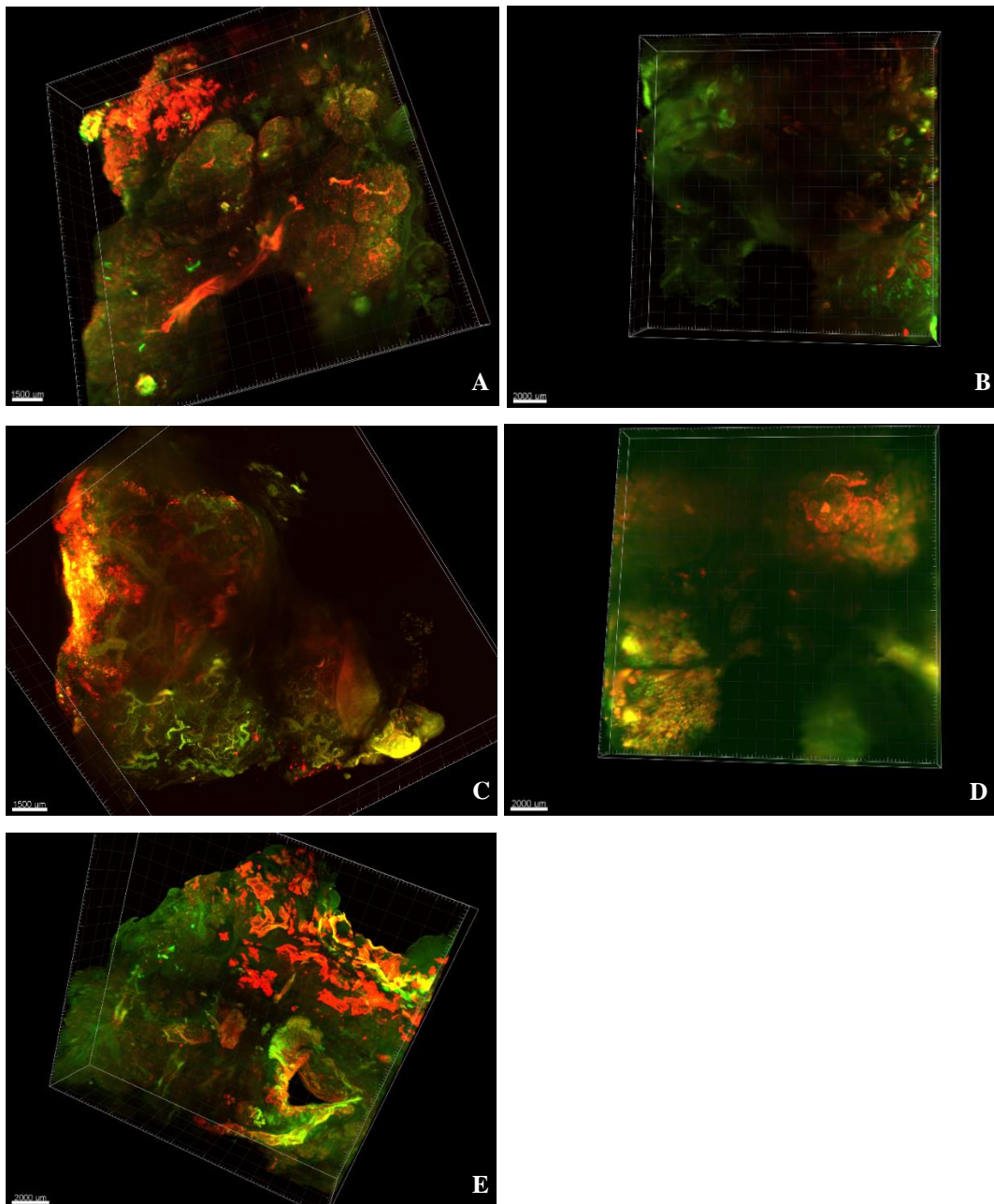


Figure 28 – 3D overview look of the multiplex with anti-CK 19 and anti-AGR2 antibodies on five samples with PDAC. After acquisition on the ultramicroscope, images were stitched with Fiji and analyzed with Imaris software. Samples stained with anti-CK 19 (red) and anti-AGR2 (green) antibodies. When co-localization of these two markers is present signal is presented as yellow. A – Sample 16. B – Sample 19. C – Sample 21. D – Sample 23. E – Sample 25 (0.63x).

AGR2 is an upregulated protein in several cancers, being associated with the metastasis process and poorer prognosis (33,34). It is localized in the endoplasmic reticulum and presents a similar structure as the disulfide isomerase, responsible for the maturation of proteins, being thought that AGR2 can also be involved in this mechanism (32–35).

Dumartin *et al.* (2011) and Ramachandran *et al.* (2008) evaluated its presence in normal pancreas, PanIN and PDAC through immunohistochemistry, describing an absence of this protein in normal pancreas but its expression in PDAC and PanIN, with exception of differentiated PDAC or with squamous differentiation (33).

Some authors support the acinar-to-ductal metaplasia as the origin of PanIN and PDAC, based on the biggest efficiency of acinar cells, compared to the ductal system, to develop PanIN, on mouse models. Ferreira *et al.* (2017) evaluated AGR2 expression in ductal and acinar-derived lesions and when present, AGR2 indicated a ductal origin (79). All five samples expressed AGR2 in PanIN and PDAC, which validates the ductal origin of the lesion, in concordance with the accepted PDAC carcinogenesis hypothesis (28).

AGR2 expression was seen in PanIN lesions and PDAC cells, as described in the literature (32–34). In some areas, AGR2 signal was also focally present in normal ducts that were in close relation with pancreatic lesions. This expression in phenotypically-normal cells was already described by Dumartin *et al.* (2017) that evaluated the expression of AGR2 in chronic pancreatitis and tubular complexes in PDAC context and found some expression in histologically normal pancreatic ducts when in close contact with PanIN, potentially representing the beginning of PDAC-initiating cells (32). Our data supports this finding. Normal ductal cells that were not connected to PanIN or PDAC didn't present this expression. Only when associated with one of these entities normal ducts presented this phenotype, which can indicate that, although histologically normal, these are not normal cells and will evolve to a PDAC-initiating cell (Figure 29).

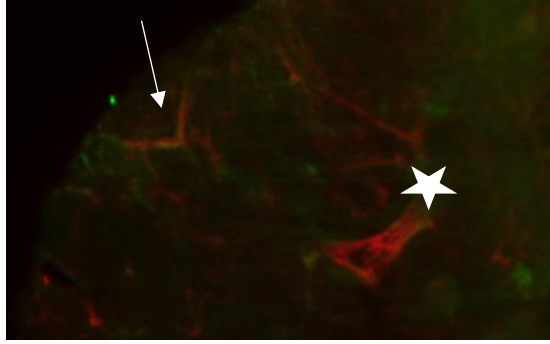


Figure 29 – 2D perspective of AGR2 expression in a phenotypically normal duct. Sample stained with anti-AGR2 (green) and anti-CK 19 (red) antibodies. AGR2 expression was found in PanIN lesions and PDAC but also in some normal-appearing ducts (arrow) that were connected to PanIN duct (star) (sample 16, 0.63x).

When analyzing all five samples it was possible to distinguish between normal ducts, PanIN and PDAC cells, but it was not possible to classify histologically different grades PanIN (Figure 30). Besides of the ductal caliber, the only visible characteristic was the cytoplasmic height, which was not enough to distinguish these structures and prohibit further analysis of spatial relationship between different grade's PanIN (Figure 31). For this distinction it would be essential to use another marker, like p53, to distinguish between low and high grade-PanIN and an image acquisition with higher magnification, fact that was not possible during the development of this thesis.

Additionally, the microscopic analysis of these finding under the confocal microscope would give us the resolution needed, although it would increase exponentially the acquisition time, due to the size and thickness of this sample, besides of needing the development of a chamber for these large size samples.

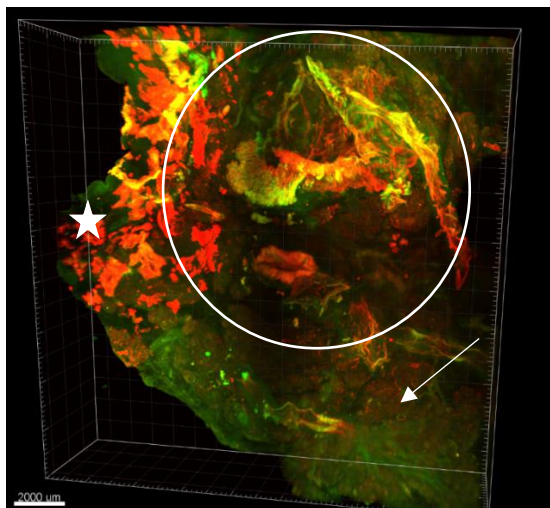


Figure 30 – 3D perspective of normal ductal component, PanIN and PDAC, stained with anti-AGR2 and anti-CK 19. Normal component (arrow), PanIN ducts (circle) and PDAC cells (star) stained with anti-AGR2 (green) and anti-CK 19 (red) antibodies (sample 25, 0.63x).

In sample 25, two ducts not physically connected in that 2 mm-thick sample, presented ductal cancerization, where an abrupt transition between an apparently normal duct and a PanIN lesion was seen. Unfortunately, due to the lack of features that could validate if this is really a transition from a phenotypically normal duct to a PanIN lesion and to which histology it would correspond, we could not explore and understand better this finding.

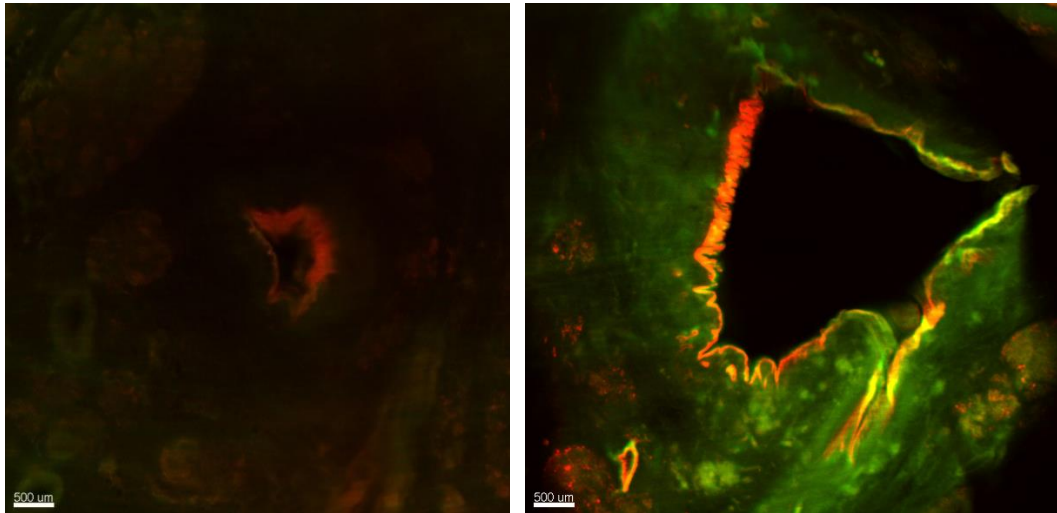


Figure 31 – 2D perspective of ductal cancerization. An abrupt transition from a phenotypically normal duct to a PanIN lesion, with enlarged cytoplasm. Although phenotypically normal, it expressed both anti-AGR2 (green) and anti-CK 19 (red) antibodies (sample 25, 0.63x).

However, it was possible to follow and understand the intricate ductal system and all its ramification and branches (Figure 32).

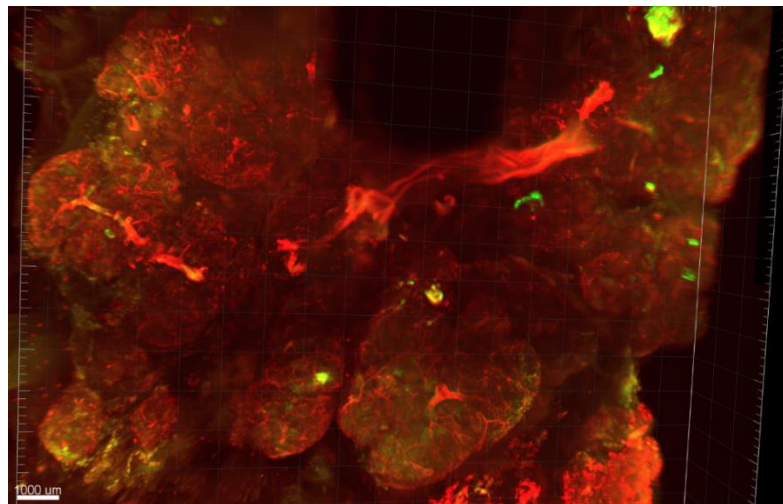


Figure 32 – 3D perspective of ductal branching. On the left we can see a ramification of a duct, stained with anti-CK 19 antibody (red). Although in this case it's not physically connected to the big duct, on the right, it seems that they could be connected (sample 16, 0.63x).

Cancer cells were present as round structures or unorganized small glandular structures. For the relationship analysis between PDAC and the remaining ductal samples, not all samples allowed convincing conclusions. However, in sample 21 we could analyze the relationship between cancer cells and the ductal system. In this sample, all ducts were connected through a 4 mm-thick central duct. Cancer cells seemed to be in close relationship with the smaller caliber ducts, through which they would invade the basement membrane. The analysis of one 5 μ m-thick section of this sample stained with HE revealed only PanIN-1. But, since no more histological analysis were made for the full thickness of this sample, we cannot assure that this duct shows only low grade PanIN in its fullness. If we were able to see that low grade PanIN is adjacent to PDAC, we would have evidence contradicting the PanINgram model for the PDAC origin. Yet, our 3D findings are not conclusive and more studies need to be done to indicate that PanIN and PDAC do not evolve independently.

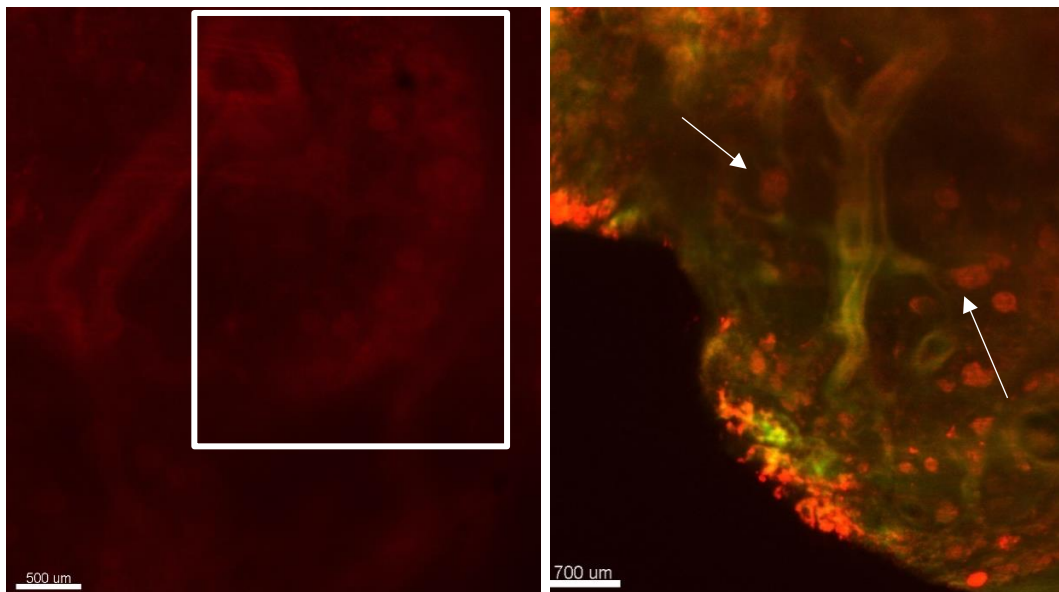


Figure 33 – 2D perspective of cancer cells in close connection to small caliber ducts, corresponding to the terminal ducts. Left image is presenting only anti-CK 19 antibody (red) expression. Right image is showing anti-CK 19 and anti-AGR2 (green) expression (sample 21, 0.63x).

4. Final Considerations and Future Goals

PDAC is one of the solid types of cancer with poorer prognosis. It is an asymptomatic disease until late stage without any early detection techniques available and limited therapeutic options by the time of diagnosis, which compromises the survival rate of the patients (6,9,15,80,81). The currently accepted progression model for PDAC is based on molecular and histological transformation in a precursor lesion, such as PanIN, but up until now, no one explored the 3D correlation of these two entities through clearing techniques.

With the goal of understanding better the spatial relationship and analyze if there is a continuum between low-grade PanIN, high-grade PanIN and PDAC, we developed the present work.

Conventional histological techniques, although valuable for diagnosis, fail in giving a 3D perspective of a sample, so needed in this case. Clearing techniques overcome this pitfall, together with light sheet microscopy, allowing the image acquisition of a cleared thick sample, their components and their spatial connections (47,53,62).

FFPE-blocks represent an interesting source of material to study several conditions, such as PanIN and PDAC, that could not be studied through conventional imaging techniques. Nevertheless, in order to analyze human samples, immunofluorescence is needed to phenotypically identify populations of interest. Up until now, maximum antibody penetration depth in cleared human FFPE blocks described is 0.6 mm (69).

FFPE archival blocks represent a precious tool of different type of samples and material. Comparing different human samples is always a challenge due to the inner variability so, in this project, we used samples with similar sizes (Appendix 3) and chose samples from the same patient whenever we needed to compare different variables, in order to lower samples' variability and ensure a valid comparison.

During the development of this thesis several protocol optimizations were made in order to increase the penetration depth of antibodies and staining's homogeneity. From all the parameters tested, the application of AR, increase of antibody supply and incubation

time, together with an enzymatic digestion of type I collagenase, proved to be essential to improve staining depth and intensity (Appendix 4).

Figure 34 summarizes the general steps that constitute the optimized protocol developed during this thesis:

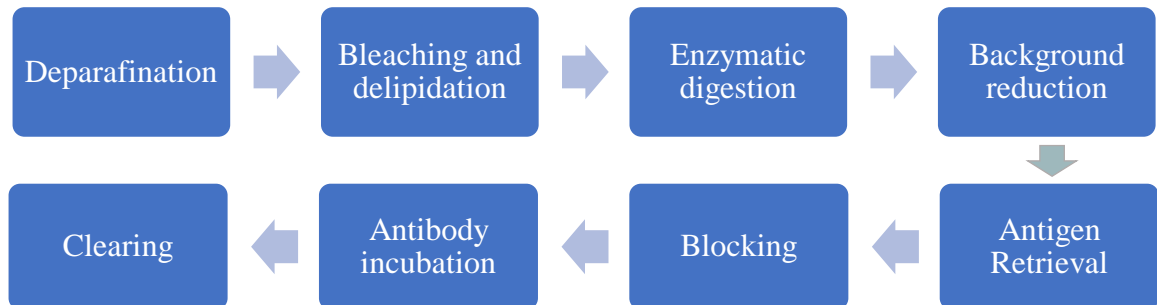


Figure 34 - Schematic workflow of the optimized protocol.

Through this protocol we were able to increase staining intensity and reduce heterogeneity, being able to image entirely a 2 mm-thick FFPE block with PDAC. From the multiplex analysis, with anti-CK19 and anti-AGR2 conjugated antibodies, we could identify normal component, PanIN and PDAC and see physical relationship between these three entities. Some evidences found during this thesis pointed to a physical connection between cancer cells and small ducts and alterations in ductal caliber and cytoplasm thickness of PanIN ducts were detected.

Unfortunately, with the development of this thesis it was not possible to elaborate about the relationship between different grades-PanIN and PDAC, as initially proposed.

First, a further technical optimization is necessary to increase staining homogeneity, which could include optimization of the antibody-antigen ratio for thick samples, comparison of the signal between direct immunolabelling and indirect immunolabelling methods or exploration of the application of other fluorophores, such as ATTO dyes. Also, application of pressure in this case should be explored to see its effect on staining speed, penetration rate and staining homogeneity. Additionally, more work needs to be done to achieve detectable nuclear staining. We were not successful with the nuclear staining of anti-p53 antibody, that could be improved through the application of enzymatic-cleaved antibodies or nanobodies, smaller in size, penetrating easier in the nuclei sided by a bigger permeabilization step. The usage of confocal imaging for

nuclear staining should be explored to understand if it could give the necessary resolution for nuclear detection.

Due to the absence of the nuclear marker, our evaluation of the ductal system was only based in the cytoplasmatic features obtained by the anti-CK 19 antibody staining, analyzed under low magnification. Restriction in time, due to the late arrival of the ultramicroscope prevented us from going further in this analysis. Although we could detect cytoplasmic alterations, we could not grade PanIN ducts due to the lack of correspondence between the 3D perspective and the conventional 2D perspective. Additional work must be developed to achieve a correspondence between the conventional histological grading system and the 3D findings. Image acquisition under the ultramicroscope at a higher magnification could also benefit this analysis, followed by the isolation of the cleared duct of interest and its posterior analysis on the confocal.

The application of this protocol to a bigger number of samples and the increase of samples' thickness would also be essential to validate the findings here reported and to ensure a correct thickness to assess ductal connections.

No problems were detected with samples' clearing methods, but it would be interesting to develop a safer immunohistochemistry and clearing protocols, with the substitution of the toxic and hazardous reagents, keeping the same results (Appendix 1).

The main advantage between clearing techniques and conventional histological techniques is the physical preservation of the sample. In order to see the viability of retrieving this sample to the FFPE blocks archival, allowing its usage for other studies, an evaluation of the morphological preservation and stability should be run in the future.

This work showed big potential in the future as a useful source of information for 3D studies. It provided a unique insight in a FFPE human block that should be explored, better understood and extended to other types of samples and pathological conditions.

5. References

1. Campbell F, Verbeke CS. Pathology of the pancreas. 1st edition. London: Springer; 2013. 3–20, 103–109, 110–150.
2. Cancer Facts & Figures. American Cancer Society. Atlanta; 2018.
3. Thun M, Linet MS, Cerhan JR, Haiman CA, Schottenfeld D. Cancer Epidemiology and prevention. Thrid Edit. Oxford University Press; 2006. 721–747.
4. Kanji ZS, Gallinger S. Diagnosis and management of pancreatic cancer. Can Med Assoc J. 2013;185(14):1219–26.
5. Kozura S, Sassa R, Taki T, Masamoto K, Nagasawa S, Saga S, et al. Relation of pancreatic duct hyperplasia to carcinoma. Cancer. 1978;43:1418–28.
6. Koorstra JM, Hustinx R, Offerhaus GJA, Maitra A. Pancreatic carcinogenesis. Pancreatology. 2008;8:110–25.
7. Weniger M, Honselmann KC, Liss AS. The extracellular matrix and pancreatic cancer : a complex relationship. Cancers. 2018;10.
8. Öhlund D, Franklin O, Lundberg E, Lundin C, Sund M. Type IV collagen stimulates pancreatic cancer cell proliferation , migration , and inhibits apoptosis through an autocrine loop. BMC Cancer. 2013;13(154):1–11.
9. Distler M, Aust D, Weitz J, Pilarsky C, Grützmann R. Precursor lesions for sporadic pancreatic cancer : PanIN , IPMN , and MCN. Biomed Res Int. 2014;1–11.
10. Kanda M, Matthaei H, Wu J, Hong S-M, Yu J, Borges M, et al. Presence of somatic mutations in most early-stage pancreatic intraepithelial neoplasia. Gastroenterology. 2012;142(4):730–3.
11. Hingorani SR, Ill EFP, Maitra A, Rajapakse V, King C, Jacobetz MA, et al. Preinvasive and invasive ductal pancreatic cancer and its early detection in the mouse. Cancer Cell. 2003;4:437–50.

12. Makohon-Moore A, Matsukuma K, Zhang M, Reiter J., Gerold J., Jiao Y, et al. Precancerous neoplastic cells can move through the pancreatic ductal system. *Nature*. 2018;561:201–5.
13. Hruban RH, Goggins M, Parsons J, Kern SE. Progression Model for Pancreatic Cancer. *Clin Cancer Res*. 2000;6:2969–72.
14. Moskaluk CA, Hruban RH, Kern SE. p16 and K-ras Gene Mutations in the Intraductal Precursors of Human Pancreatic Adenocarcinoma. *Cancer Res*. 1997;57:2140–3.
15. Ottenhof NA, Milne ANA, Morsink FHM, Drilenburg P, Kate FJW, Maitra A, et al. Pancreatic intraepithelial neoplasia and pancreatic tumorigenesis of mice and men. *Arch Pathol Lab Med*. 2003;133:375–81.
16. Hruban R, Adsay N, Albores-Saavedra J, Compton C, Garrett E, Goodman S, et al. Pancreatic intraepithelial neoplasia: a new nomenclature and classification system for pancreatic duct lesions. *Am J Surg Pathol*. 2001;25(5):579–86.
17. Pittman ME, Rao R, Hruban RH. Classification, morphology, molecular pathogenesis, and outcome of premalignant lesions of the pancreas. *Arch Pathol Lab Med*. 2017;141:1606–14.
18. Koorstra JM, Feldmann G, Habbe N, Maitra A. Morphogenesis of pancreatic cancer : role of pancreatic intraepithelial neoplasia (PanINs). *Langenbecks Arch Surg*. 2008;393(4):561–70.
19. Shen R, Wang Q, Cheng S, Liu T, Jiang H, Zhu J, et al. The biological features of PanIN initiated from oncogenic Kras mutation in genetically engineered mouse models. *Cancer Lett*. 2013;339:135–43.
20. Basturk O, Hong S, Wood L, Adsay N, Albores-Saavedra J, Baikin A, et al. A revised classification system and recommendations from the baltimore consensus meeting for neoplastic precursor lesions in the pancreas. *Am J Surg Pathol*. 2015;39(12):1730–41.
21. Esposito I, Konukiewitz B, Schlitter AM, Klöppel G. Pathology of pancreatic ductal adenocarcinoma : Facts , challenges and future developments. *World J*

- Gastroenterol. 2014;20(38):13833–41.
22. Wilentz RE, Iacobuzio-donahue CA, Argani P, Mccarthy DM, Parsons JL, Yeo CJ, et al. Loss of expression of DPC4 in pancreatic intraepithelial neoplasia : evidence that DPC4 inactivation occurs late in neoplastic progression. *Cancer Res.* 2000;60:2002–6.
 23. Bardeesy N, Aguirre AJ, Chu GC, Cheng K, Lopez L V, Hezel AF, et al. Both p16 Ink4a and the p19 Arf -p53 pathway constrain progression of pancreatic adenocarcinoma. *PNAS.* 2006;103(15):5947–52.
 24. Bardeesy N, Depinho RA. Pancreatic cancer biology and genetics. *Nat Rev Cancer.* 2002;2:897–909.
 25. Guo J, Xie K, Zheng S. Molecular biomarkers of pancreatic intraepithelial neoplasia and their implications in early diagnosis and therapeutic intervention of pancreatic cancer. *Int J Biol Sci.* 2016;12(3):292–301.
 26. Hruban RH, Mansfeld ADM Van, Offerhaus GJA, Weering DHJ Van, Allison DC, Goodman SN, et al. K-ras oncogene activation in adenocarcinoma of the human pancreas. *Am J Pathol.* 1993;143(2):545–54.
 27. Redston MS, Caldas C, Seymour AB, Hruban RH, Costa L, Yeo CJ, et al. p53 mutations in pancreatic carcinoma and evidence of common involvement of homocopolymer tracts in DNA microdeletions. *Cancer Res.* 1994;54:3025–33.
 28. Feldmann G, Beaty R, Hruban RH., Maitra A. Molecular genetics of pancreatic intraepithelial neoplasia. *J Hepatobiliary Pancreat Surg.* 2009;14(3):224–32.
 29. Heek NT van, Meeker AK, Kern SE, Yeo CJ, Lillemoe KD, Cameron JL, et al. Telomere shortening is nearly universal in pancreatic intraepithelial neoplasia. *Am J Pathol.* 2002;161(5):1541–7.
 30. Fukushima N, Sato N, Ueki T, Rosty C, Walter KM, Wilentz RE, et al. Aberrant Methylation of Preproenkephalin and p16 Genes in Pancreatic Intraepithelial Neoplasia and Pancreatic Ductal Adenocarcinoma. *Am J Pathol.* 2002;160(5):1573–81.

31. Schutte M, Hruban RH, Geradts J, Maynard R, Hilgers W, Rabindran SK, et al. Abrogation of the Rb/p16 tumor-suppressive pathway in virtually all pancreatic carcinomas. *Cancer Res.* 1997;57:3126–31.
32. Dumartin L, Alrawashdeh W, Trabulo SM, Radon TP, Steiger K, Feakins RM, et al. ER stress protein AGR2 precedes and is involved in the regulation of pancreatic cancer initiation. *Oncogene.* 2017;36:3094–103.
33. Dumartin L, Whiteman HJ, Weeks ME, Hariharan D, Dmitrovic B, Iacobuzio-donahue CA, et al. AGR2 is a novel surface antigen that promotes the dissemination of pancreatic cancer cells through regulation of cathepsins B and D. *Tumor stem cell Biol.* 2011;77(22):7091–102.
34. Norris AM, Gore A, Balboni A, Young A, Longnecker DS, Korc M. AGR2 is a SMAD4-suppressible gene that modulates MUC1 levels and promotes the initiation and progression of pancreatic intraepithelial neoplasia. *Oncogene.* 2012;32:3867–76.
35. Ramachandran V, Arumugan T, Wang H, Logsdon CD. Anterior gradient 2 is expressed and secreted during the development of pancreatic cancer and promotes cancer cell survival. *Cancer Res.* 2008;68(19):7811–8.
36. Sitek B, Sipos B, Alkatout I, Poschmann G, Stephan C, Schulenburg T, et al. Analysis of the pancreatic tumor progression by a quantitative proteomic approach and immunohistochemical validation. *J Proteome Res.* 2009;8(4):1647–56.
37. Matsuyama M, Kondo F, Ishihara T. Evaluation of pancreatic intraepithelial neoplasia and mucin expression in normal pancreata. *J Hepatobiliary Pancreat Sci.* 2012;19(3):242–8.
38. Biankin A V, Kench JG, Morey AL, Lee C, Biankin SA, Head DR, et al. Overexpression of p21 WAF1 / CIP1 is an early event in the development of pancreatic intraepithelial neoplasia. *Cancer Res.* 2001;61(24):8830–7.
39. Zinzuk J, Zareba K, Guzinska-Ustymowicz K, Kendra B, Kemon A, Pryczynicz A. p16 , p21 , and p53 proteins play an important role in development

- of pancreatic intraepithelial neoplastic. *Ir J Med Sci.* 2018;187(3):629–37.
40. Makohon-Moore AP, Matsukuma K, Zhang M, Reiter JG, Gerold JM, Jiao Y, et al. Precancerous neoplastic cells can move through the pancreatic ductal system. *Nature.* 2017;561:201–5.
 41. Rozenbium E, Schutte M, Goggins M, Hahn SA, Panzer S, Zahurak M, et al. Tumor-suppressive pathways in pancreatic carcinoma. *Cancer Res.* 1997;57(9):1731–5.
 42. Taii A, Hamada S, Kataoka PK, Yasukawa S. Correlations between p53 gene mutations and histologic characteristics of pancreatic ductal carcinoma. *Pancreas.* 2009;38(2):60–7.
 43. Garcia-carracedo D, Yu C, Akhavan N, Fine SA. Smad4 loss synergizes with TGF α overexpression in promoting pancreatic development, PanIN development, and fibrosis. *PLoS One.* 2015;10(3):1–17.
 44. Yokode M, Akita M, Fujikura K, Kim M, Morinaga Y, Yoshikawa S, et al. High-grade PanIN presenting with localised stricture of the main pancreatic duct: A clinicopathological and molecular study of 10 cases suggests a clue for the early detection of pancreatic cancer. *Histopathology.* 2018;73:247–58.
 45. Hosoda W, Chianchiano P, Griffin JF, Pittman ME, Yu J, Shindo K, et al. Genetic analyses of isolated high-grade pancreatic intraepithelial neoplasia (HG-PanIN) reveal paucity of alterations in TP53 and SMAD4. *J Pathol.* 2017;242(1):16–23.
 46. Maitra A, Adsay V, Aragni P, Iacobuzio-donahue C, Marzo A De, Cameron JL, et al. Multicomponent analysis of the pancreatic adenocarcinoma progression model using a pancreatic intraepithelial neoplasia tissue microarray. *Mod Pathol.* 2003;16(9):902–12.
 47. Hong S, Noë M, Hruban CA, Thompson ED, Wood LD, Hruban RH. A “ clearer ” view of pancreatic pathology: a review of tissue clearing and advanced microscopy techniques. *Adv Anat Pathol.* 2019;26:31–9.
 48. Murray E, Cho JH, Goodwin D, Ku T, Swaney J, Kim S, et al. Simple, scalable

- proteomic imaging for high-dimensional profiling of intact systems. 2015;163(6):1500–14.
49. Susaki EA, Ueda HR. Whole-body and whole-organ clearing and imaging techniques with single-cell resolution : toward organism-level systems biology in mammals. *Cell Chem Biol.* 2016;23:137–57.
 50. Lee E, Choi J, Jo Y, Kim JY, Jang YJ, Lee HM, et al. ACT-PRESTO : Rapid and consistent tissue clearing and labeling method for 3-dimensional (3D) imaging. *Sci Rep.* 2016;6.
 51. Pan C, Cai R, Quacquarelli FP, Ghasemigharagoz A, Loubopoulos A, Matryba P, et al. Shrinkage-mediated imaging of entire organs and organisms using uDISCO. *Nat Methods.* 2016;13(10).
 52. Perbellini F, Liu AKL, Watson SA, Bardi I, Stephen M, Terracciano CM. Free-of-Acrylamide SDS-based Tissue Clearing (FASTClear) for three dimensional visualization of myocardial tissue. *Nature.* 2017;7:1–9.
 53. Richardson D, Lichtman J. Clarifying tissue clearing. *Cell.* 2015;162(2):246–57.
 54. Cai R, Pan C, Ghasemigharagoz A, Todorov MI, Zhao S, Bhatia HS, et al. Panoptic vDISCO imaging reveals neuronal connectivity , remote trauma effects and meningeal vessels in intact transparent mice. *Cold Spring Harb Lab.* 2018;1–29.
 55. Hahn C, Becker K, Saghafi S, Pende M, Foroughipour M, Heinz DE, et al. High-resolution imaging of fluorescent whole mouse brains using stabilised organic media (sDISCO). *J Biophotonics.* 2019;12(8):1–29.
 56. Lui A, Lai H, Chang R, Gentleman S. Free of acrylamide sodium dodecyl sulphate(SDS)-based tissue clearing (FASTClear): anovel protocol of tissue clearing forthree-dimensional visualization of humanbrain tissues. *Neuropathol Appl Neurobiol.* 2017;43:346–51.
 57. Tomer R, Ye L, Hsueh B, Deisseroth K. Advanced CLARITY for rapid and high-resolution imaging of intact tissues. *Nature.* 2014;9(7):1682–97.






58. Tainaka K, Kuno A, Kubota SI, Murakami T, Ueda HR. Chemical principles in tissue clearing and staining protocols for whole-body cell profiling. *Annu Rev Cell Dev Biol.* 2016;32:713–41.
59. Ertürk A, Becker K, Jährling N, Mauch CP, Hojer CD, Egen JG, et al. Three-dimensional imaging of solvent-cleared organs using 3DISCO. *Nature.* 2012;7(11):1983–95.
60. Kubota SI, Takahashi K, Nishida J, Tainaka K, Miyazono K, Ueda HR, et al. Whole-body profiling of cancer metastasis with single-cell resolution. *Cell Rep.* 2017;20:236–50.
61. Mauch CP, Dodt H, Leischner U, Schierloh A, Ja N, Becker K, et al. Ultramicroscopy: three-dimensional visualization of neuronal networks in the whole mouse brain. *Nat Methods.* 2007;4(4):331–6.
62. Azaripour A, Lagerweij T, Scharfbillig C, Jadcak E, Willershausen B, Noorden CJF Van. A survey of clearing techniques for 3D imaging of tissues with special reference to connective tissue. *Prog Histochem Cytochem.* 2016;51(2):9–23.
63. Klingberg A, Hasenberg A, Ludwig-Portugall I, Medyukhina A, Männ L, Brenzel A, et al. Fully automated evaluation of total glomerular number and capillary tuft size in nephritic kidneys using lightsheet microscopy. *J Am Soc Nephrol.* 2017;28(2):452–9.
64. Silvestri L, Costantini I, Sacconi L, Pavone FS. Clearing of fixed tissue: a review from a microscopist's perspective. *J Biomed Opt.* 2016;21(8).
65. Tainaka K, Kubota SI, Suyama TQ, Susaki EA, Perrin D, Ukai-tadenuma M, et al. Whole-body imaging with single-cell resolution by tissue decolorization. *Cell.* 2014;159:911–24.
66. Ramos-Vara JA. Technical aspects of immunohistochemistry. *Vet Pathol.* 2005;42(4):405–26.
67. Kim S, Hun J, Murray E, Bakh N, Choi H, Ohn K, et al. Stochastic electrotransport selectively enhances the transport of highly electromobile molecules. *Proc Natl Acad Sci U S A.* 2015;112(46).





68. Renier N, Wu Z, Simon DJ, Yang J, Ariel P, Tessier-lavigne M. iDISCO : A simple , mapid method to immunolabel large tissue samples for volume imaging. *Cell*. 2014;159:896–910.
69. Noë M, Rezaee N, Asrani K, Skaro M, Groot VP, Wu P, et al. Immunolabeling of cleared human pancreata provides insights into three-dimensional pancreatic anatomy and pathology. *Am J Pathol*. 2018;1–7.
70. Treweek JB, Chan KY, Flytzanis NC, Yang B, Greenbaum A, Lignell A, et al. Whole-body tissue stabilization and selective extractions via tissue-hydrogel hybrids for high-resolution intact cricuit mapping and phenotyping. *Nat Protoc*. 2015;10(11):1860–96.
71. Saritas T, Puelles VG, Su X, McCormick JA, Welling PA, Ellison DH, et al. Optical clearing in the kidney reveals potassium-mediated tubule remodeling. *Cell Reports*. 2018;25(10):2668–75.
72. Lai HM, Lui AKL, Ng HHM, Goldfinger MH, Chau TW, Defelice J, et al. Next generation histology methods for three- dimensional imaging of fresh and archival human brain tissues. *Nat Commun*. 2018;9.
73. Du H, Hou P, Wang L, Wang Z, Li Q. Modified CLARITY achieving faster and better intact mouse brain clearing and immunostaining. *Sci Rep*. 2019;9:1–11.
74. Poola PK, Afzal IM, Yoo Y, Kim KH, Chung E. Light sheet microscopy for histopathology applications. *Biomed Eng Lett*. 2019;24(9):279–91.
75. Albert-smet I, Marcos-vidal A, Vaquero JJ, Desco M, Muñoz-barrutia A, Ripoll J. Applications of light-sheet microscopy in microdevices. *Front Neuroanat*. 2019;13:1–15.
76. Bannas P, Hambach J, Koch-Nolte F. Nanobodies and nanobody-based human heavy chain antibodies as antitumor therapeutics. *Front Immunology*. 2017;8:1–13.
77. Digiuseppe JA, Hruban RH, Goodman SN, Polak M, Berg FM, Allison DC, et al. Overexpression of p53 protein in adenocarcinoma of the pancreas. *Anat Pathol*. 1993;101:684–8.

78. Rawla P, Sunkara T, Gaduputi V. Epidemiology of pancreatic cancer : global trends , etiology and risk factors. *World J Oncol.* 2019;10(1):10–27.
79. Ferreira RMM, Sancho R, Messal HA, Rosewell I, Quaglia A, Behrens A. Duct- and acinar-derived pancreatic ductal adenocarcinomas show distinct tumor progression and marker xpression. *Cell Reports.* 2017;21:966–78.
80. Yonezawa S, Higashi M, Yamada N, Goto M. Precursor lesions of pancreatic cancer. *Gut Liver.* 2008;2(3):137–54.
81. Hruban RH, Maitra A, Goggins M. Update on pancreatic intraepithelial neoplasia. *Int J Clin Exp Pathol.* 2008;1:306–16.

6. Appendix

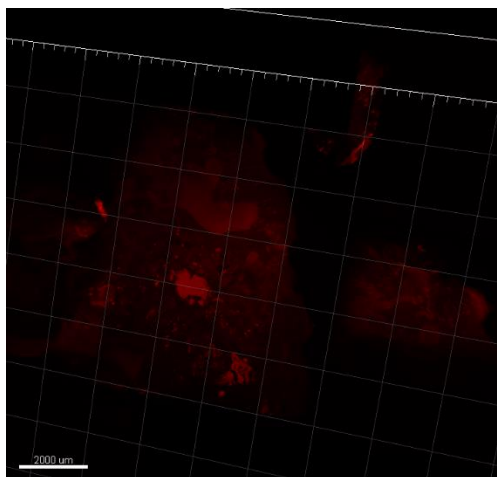
6.1 - Appendix 1 - Risk assessment of reagents

Reagent	Hazard Statement	Label elements
1x PBS	-	-
AR solution	-	-
BSA	H302-Harmful if swallowed.	
DBE	H400-Very toxic to aquatic life. H410-Very toxic to aquatic life with long lasting effects.	
Dichloromethane	H351-Suspected of causing cancer. H315-Causes skin irritation. H319-Causes serious eye irritation. H336-May cause drowsiness or dizziness	
DMSO	H227-Combustible liquid.	
ECi	-	-
Heparin	-	-
Hydrogen peroxide	H318-Causes serious eye damage. H302-Harmful if swallowed.	
Methanol	H225-Highly flammable liquid and vapor. H301-Toxic if swallowed.	

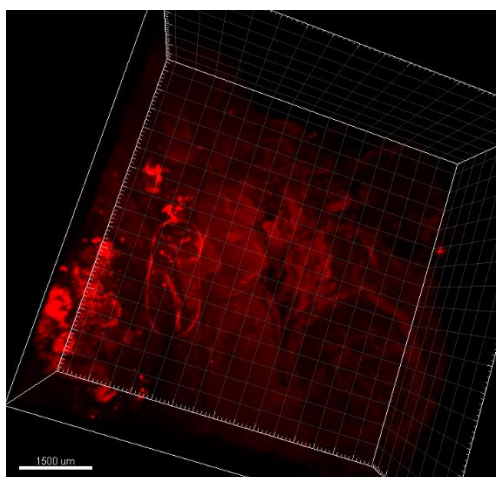
	<p>H311-Toxic in contact with skin.</p> <p>H331-Toxic if inhaled.</p> <p>H370-Causes damage to organs.</p>	
Sodium azide	<p>H300-Fatal if swallowed.</p> <p>H410-Very toxic to aquatic life with long lasting effects.</p>	
Triton X-100	<p>H302 - Harmful if swallowed</p> <p>H318-Causes serious eye damage</p> <p>H411 - Toxic to aquatic life with</p>	
Tween-20	-	-
Type I collagenase	<p>H315-Causes skin irritation.</p> <p>H319-Causes serious eye irritation.</p> <p>H334-May cause allergy or asthma symptoms or breathing difficulties if inhaled.</p> <p>H335-May cause respiratory irritation.</p>	
Xylene	<p>H226-Flammable liquid and vapor.</p> <p>H312-Harmful in contact with skin.</p> <p>H315-Causes skin irritation.</p> <p>H332-Harmful if inhaled.</p>	

6.2 - Appendix 2 - Samples with enzymatic digestion

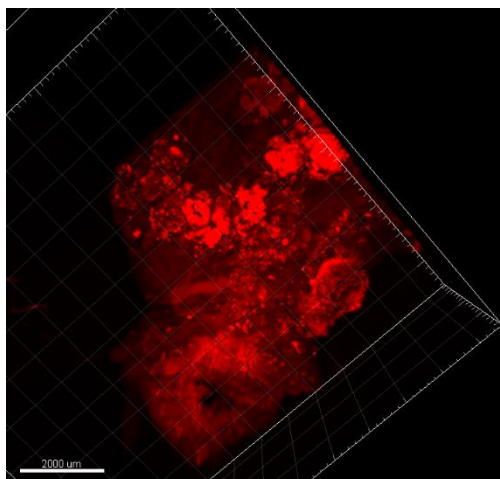
Sample 11 – Control sample incubated in 1x PBS during enzymatic digestion before glycine.



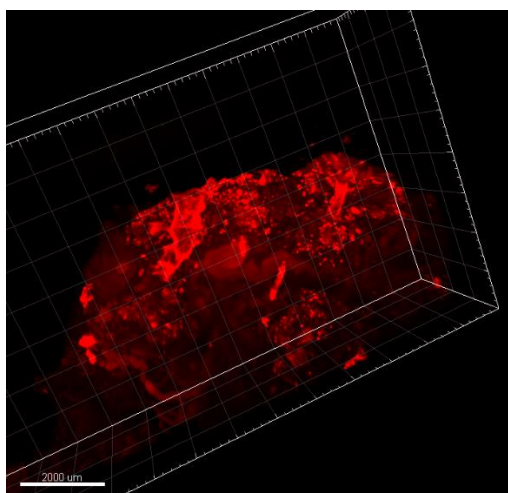
Sample 11 – Control sample incubated in 1x PBS during enzymatic digestion after blocking.



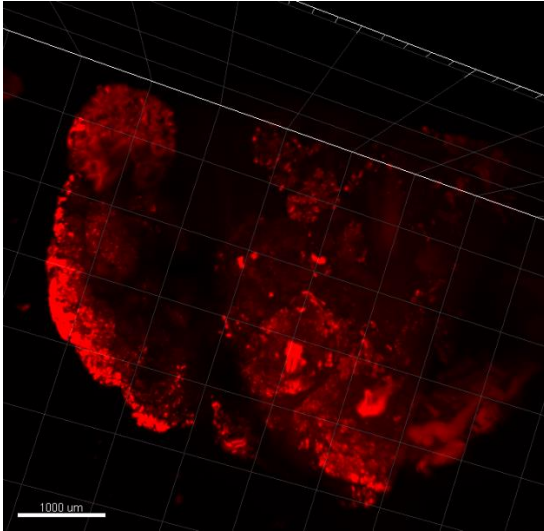
Sample 12 – Type I collagenase for 1 hour before glycine.



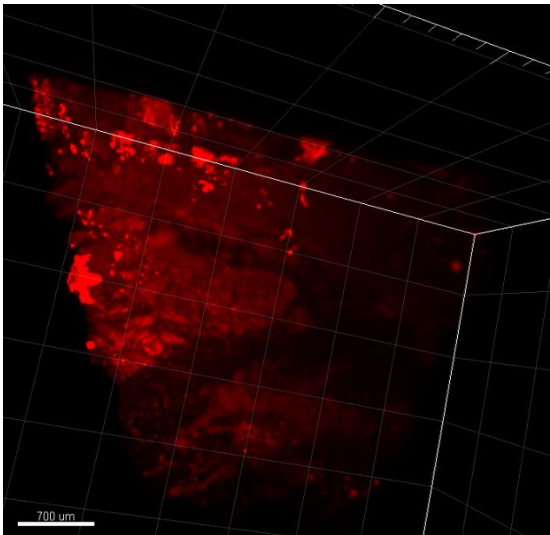
Sample 12 – Type I collagenase for 3 hours before glycine.



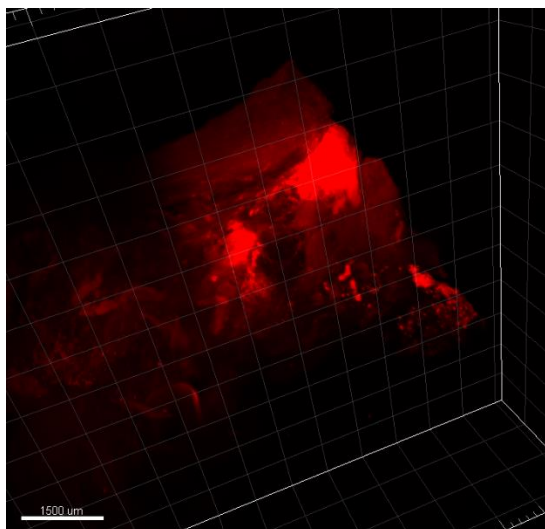
Sample 13 – Type IV collagenase for 1 hour before glycine.



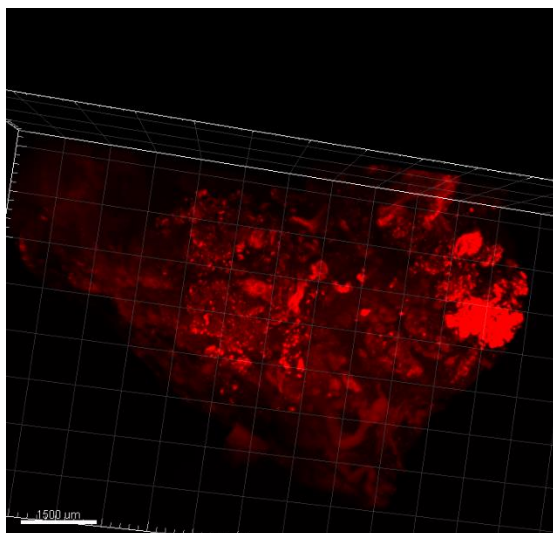
Sample 13 – Type IV collagenase for 3 hours before glycine.



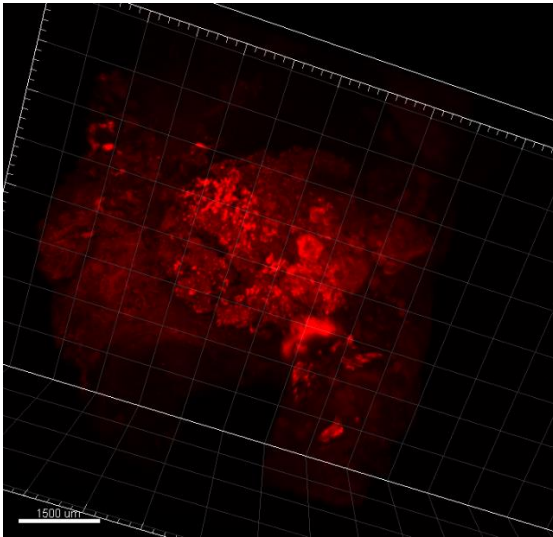
Sample 14 – Type I and IV collagenase for 1 hour before glycine.



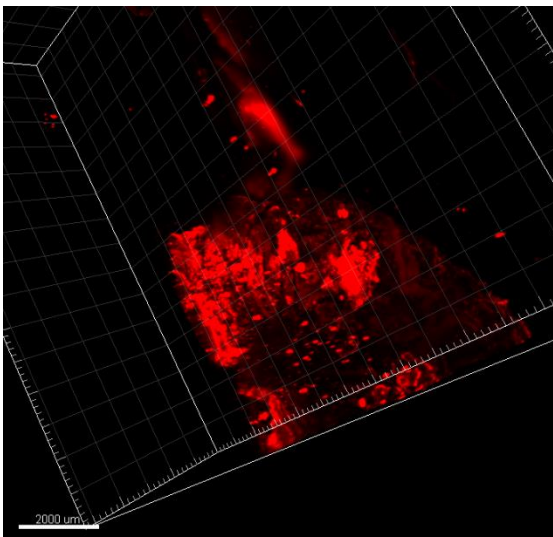
Sample 14 – Type I and IV collagenase for 3 hours before glycine.



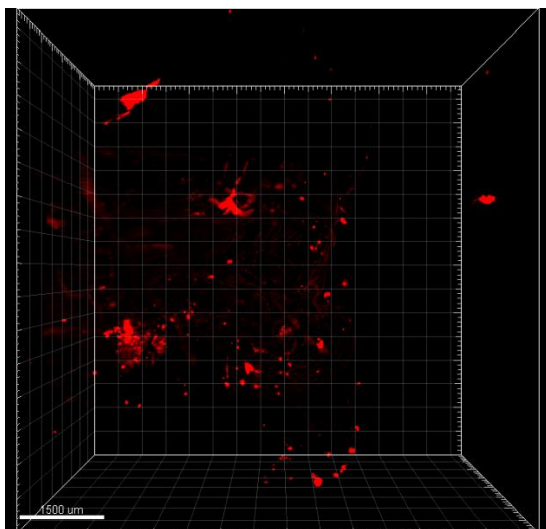
Sample 35 – Type I collagenase for 1 hour after blocking.



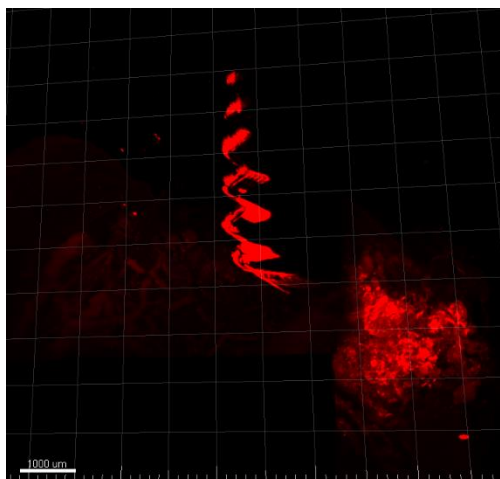
Sample 35 – Type I collagenase for 3 hours after blocking.



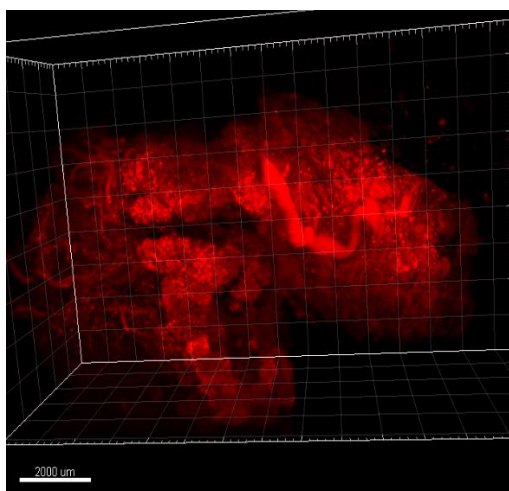
Sample 36 – Type IV collagenase for 1 hour after blocking.



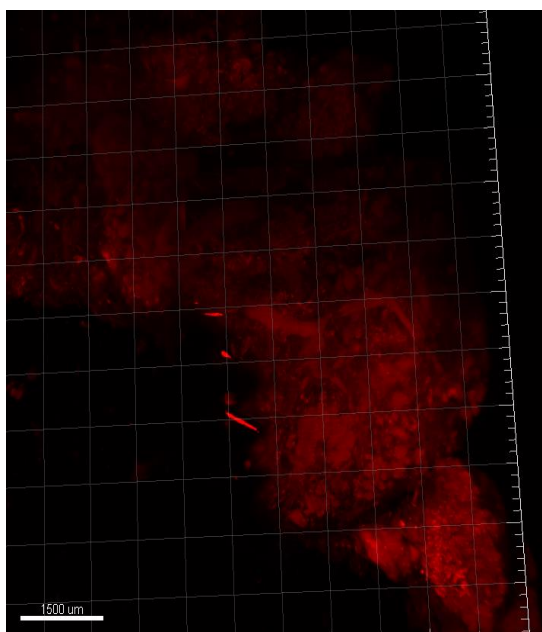
Sample 36 – Type IV collagenase for 3 hours after blocking.



Sample 37 – Type I and IV collagenase for 1 hour after blocking.



Sample 37 – Type I and IV collagenase for 3 hours after blocking.



6.3 - Appendix 3 – Sample's dimension

Sample ID	Dimension (cm) – length x height	Thickness (mm)
Sample 4	1.5 x 1	1.5
Sample 5	1.5 x 1	1.5
Sample 6	1.4 x 1.5	2
Sample 8	2.5 x 1.6	2
Sample 9	2.5 x 1	2
Sample 10	1.9 x 1.8	2
Sample 11	2.4 x 1.5	1.5
Sample 12	1.8 x 1	2
Sample 13	2 x 1.5	1.5
Sample 14	2 x 1.1	1.5
Sample 16	2.5 x 2	2
Sample 19	1.9 x 1.8	3
Sample 21	1.8 x 1.5	3
Sample 23	2.3 x 1.7	1.5
Sample 25	2 x 2.2	3
Sample 35	2.3 x 1.5	1.5
Sample 36	2.2 x 1.5	2
Sample 37	2.8 x 1.6	2
Sample 40	2.5 x 1.9	2
Sample 43	2.3 x 2	2

6.4 - Appendix 4 – Deep immunolabelling of FFPE with PDAC

1. Place FFPE block in the oven at 72°C for 30 min (if need extend time until all paraffin is melted).
2. Place sample in xylene for 2 days, with shaking at 37°C.
 - a. Solution should be refreshed twice per day.
 - b. PAUSE POINT: If needed, the incubation time could be extended without damage of tissue.
3. Wash 3 x 1 hour in methanol 100, with shaking at RT.
4. Wash for 1 hour in methanol 100, without shaking at 4°C.
5. Incubate overnight in 66% DCM/33 % methanol, shaking at RT.
 - a. Note: When placed in this solution sample will float but it'll sink during incubation time.
6. Wash twice in 100% methanol.
7. Incubate overnight in 5% hydrogen peroxide/ methanol, with shaking at RT.
8. Wash for 20 min in 1x PBS, shaking at room temperature.
 - a. Note: Sample will float so a compress can be added to make sure it sinks and hydration is complete.
 - b. PAUSE POINT: If necessary, sample can be left in this solution. To prevent fungus contamination, add 0.1% sodium azide.
9. Wash for 1 hour in 1x PBS/ 0.2% triton X-100 (PBS-T 0.2%), shaking at room temperature.
10. Wash for 5 min in 1x PBS.
11. Incubate for 1 hour in type I collagenase (1mg/mL), shaking at 37° C.
 - a. CRITICAL POINT: Time can be extended depending on sample's size, but over-treatment can cause desegregation and loss of normal consistency and morphology.
12. Place sample for 20 min in pre-cold PBS, without shaking at 4°C.
13. Wash 15 min in 1x PBS, shaking at room temperature.
14. Incubate for 2 days in 20% DMSO/ 0.3 mol/L glycine/ PBS – T 0.2%, shaking at 37°C.
15. Incubate for 24 hours in AR solution pH9, shaking at 37°C.

- a. Note: Solution's pH must be defined according to the antibody used. Validation of AR should be done previously in a 5 μm -thick slice from a positive control.
16. Pre-heat AR solution in the steamer (90°C) for 30 min.
17. Place sample in the AR solution for 40 min.
 - a. CRITICAL POINT: AR incubation time must be optimized accordingly to the sample's size. But if over-extended it could cause loss of integrity.
18. Wash briefly in PBS-T 0.2%.
19. Block for 2 days in 10% DMSO/ 6% BSA/ 0.1 % sodium azide/ PBS-T 0.2%, shaking at 37°C.
20. Wash 2x 1 hour in 1x PBS/ 0.2% Tween 20 / heparin 10 $\mu\text{g}/\text{mL}$ (0.2% PBS-Th).
21. Incubate for 7 days with conjugated antibody in 0.2% PBS-Th/ 5% DMSO/ 3% BSA/ 0.1% sodium azide, shaking at 37°C.
 - a. From this moment, protect you sample from light.
 - b. On the third day add the same amount of antibody as added in the first day, without changing the diluent.
22. Wash 5 x 1 hour in 0.2% PBS-Th, shaking at room temperature.
 - a. PAUSE POINT: Protocol can be paused here. Store sample at 4°C and add 0.1% sodium azide to prevent fungus contamination.
23. Dehydrate in increasing grade of methanol, shaking at room temperature:
 - a. 45 min in 70% methanol.
 - b. 45 min in 96% methanol.
 - c. 30 min in 100% methanol.
 - d. 30 min in 100% methanol.
 - e. 1 hour in 100% methanol.
24. Incubated for 3 hours in 66% DCM/33 % methanol, without shaking RT.
25. Incubate for 15 min in DCM.
26. Place sample in DBE until cleared.